

AD-A085 806

AEROSPACE CORP EL SEGUNDO CA ENGINEERING GROUP  
ONE- AND TWO-PHASE NOZZLE FLOWS. (U)  
JAN 80 I CHANG

F/G 21/8.2

UNCLASSIFIED

TR-0080(5901-01)-1

SD-TR-80-26

F04701-79-C-0080

NL

1 of 1

20

20/01/80

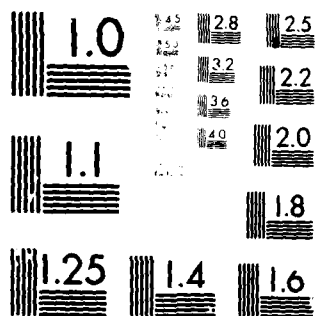
END

DATE

FILED

7-80

DTIC



MICROCOPY RESOLUTION TEST CHART  
NATIONAL BUREAU OF STANDARDS-1963-A

**LEVEL** *II*

*12*

ADA 085806

## One-and-Two-Phase Nozzle Flows

I. SHIH CHANG  
Engineering Group  
The Aerospace Corporation  
El Segundo, Calif. 90245

31 January 1980

DTIC  
ELECTE  
JUN 19 1980  
S D C

Final Report

APPROVED FOR PUBLIC RELEASE;  
DISTRIBUTION UNLIMITED

80 6 18 0 10

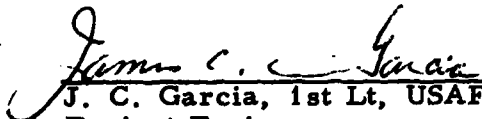
Prepared for  
SPACE DIVISION  
AIR FORCE SYSTEMS COMMAND  
Los Angeles Air Force Station  
P.O. Box 92980, Worldway Postal Center  
Los Angeles, Calif. 90009

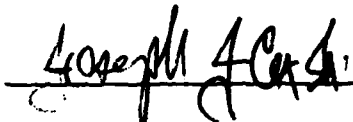
DDC FILE COPY

This final report was submitted by The Aerospace Corporation, El Segundo, CA 90245, under Contract F04701-79-C-0080 with the Space Division, Deputy for Space Communications Systems, P.O. Box 92960, Worldway Postal Center, Los Angeles, CA 90009. It was reviewed and approved for The Aerospace Corporation by E. G. Hertler, Engineering Group. First Lieutenant J. C. Garcia, YLXT was the Deputy for Technology project engineer.


This report has been reviewed by the Public Affairs Office (PAS) and is releasable to the National Technical Information Service (NTIS). At NTIS, it will be available to the general public, including foreign nations.

This technical report has been reviewed and is approved for publication. Publication of this report does not constitute Air Force approval of the report's findings or conclusions. It is published only for the exchange and stimulation of ideas.

  
J. C. Garcia, 1st Lt, USAF  
Project Engineer

  
Joseph J. Cox, Jr., Lt Col, USAF  
Chief, Advanced Technology Division

FOR THE COMMANDER

  
Burton H. Holaday, Col, USAF  
Director of Technology Plans  
and Analysis

UNCLASSIFIED

SECURITY CLASSIFICATION OF THIS PAGE (When Data Entered)

REPORT DOCUMENTATION PAGE		READ INSTRUCTIONS BEFORE COMPLETING FORM
1. REPORT NUMBER <b>18</b> SD-TR-80-26	2. GOVT ACCESSION NO. AD-A085 806	3. RECIPIENT'S CATALOG NUMBER
4. TITLE (and Subtitle) <b>6</b> ONE- AND TWO-PHASE NOZZLE FLOWS		5. TYPE OF REPORT & PERIOD COVERED <b>9</b> Final rept. Jan. 1978-Jan. 1980
7. AUTHOR(s) <b>10</b> I-Shih Chang		6. PERFORMING ORGANIZATION NUMBER <b>14</b> TR-0080(5901-01)-1
9. PERFORMING ORGANIZATION NAME AND ADDRESS The Aerospace Corporation El Segundo, Calif. 90245		8. CONTRACT OR GRANT NUMBER(s) <b>15</b> F04701-79-C-0080
11. CONTROLLING OFFICE NAME AND ADDRESS Space Division Air Force Systems Command Los Angeles, Calif. 90009		10. PROGRAM ELEMENT, PROJECT, TASK AREA & WORK UNIT NUMBERS
12. REPORT DATE <b>11</b> 31 January 1980		13. NUMBER OF PAGES 64
14. MONITORING AGENCY NAME & ADDRESS (if different from Controlling Office) <b>12</b> 64		15. SECURITY CLASS. (of this report) Unclassified
		15a. DECLASSIFICATION/DOWNGRADING SCHEDULE
16. DISTRIBUTION STATEMENT (of this Report)  Approved for public release; distribution unlimited		
17. DISTRIBUTION STATEMENT (of the abstract entered in Block 20, if different from Report)		
18. SUPPLEMENTARY NOTES		
19. KEY WORDS (Continue on reverse side if necessary and identify by block number) Gas-particle Two-phase Nozzle Transonic Flow Computational Method		
20. ABSTRACT (Continue on reverse side if necessary and identify by block number) A time-dependent technique, in conjunction with the boundary-fitted coordinates system, is applied to solve a gas-only one-phase flow and a fully-coupled, gas-particle two-phase flow inside nozzles with small throat radii of curvature, steep wall gradients, and submerged configurations. The emphasis of the study has been placed on one- and two-phase flow in the transonic region. Various particle sizes and particle mass fractions have been		

DD FORM 1473  
(7/73)

411279

UNCLASSIFIED

SECURITY CLASSIFICATION OF THIS PAGE (When Data Entered)

UNCLASSIFIED

SECURITY CLASSIFICATION OF THIS PAGE(When Data Entered)

19. KEY WORDS (Continued)

20. ABSTRACT (Continued)

investigated in the two-phase flow. The salient features associated with the two-phase nozzle flow compared with those of the one-phase flow are illustrated through the calculations for a JPL nozzle configuration, for the Titan III solid rocket motor nozzle, and for the submerged nozzle configuration utilized in the Inertial Upper Stage (IUS) solid rocket motor.

UNCLASSIFIED

SECURITY CLASSIFICATION OF THIS PAGE(When Data Entered)

## PREFACE

The author is indebted to the late Dr. John Vasiliu for his review of this report and for his encouragement and helpful suggestions throughout the study.

Accession For	
NTIS GRA&I	<input checked="checked" type="checkbox"/>
DDC TAB	<input type="checkbox"/>
Unannounced	<input type="checkbox"/>
Justification	
By _____	
Distribution/	
Availability Codes	
Dist	Avail and/or special
A	

## CONTENTS

PREFACE . . . . .	1
I. INTRODUCTION . . . . .	7
II. GOVERNING EQUATIONS . . . . .	11
III. NUMERICAL ASPECTS . . . . .	17
IV. NOZZLE WITH SMALL THROAT RADIUS OF CURVATURE--JPL NOZZLE . . . . .	23
A. One-Phase Flow . . . . .	23
B. Two-Phase Flow . . . . .	26
V. NOZZLE WITH VERY STEEP ENTRANCE-- TITAN III MOTOR . . . . .	41
A. One-Phase Flow . . . . .	41
B. Two-Phase Flow . . . . .	45
VI. SUBMERGED NOZZLE--IUS SMALL MOTOR . . . . .	51
A. One-Phase Flow . . . . .	51
B. Two-Phase Flow . . . . .	54
VII. CONCLUDING REMARKS . . . . .	61
REFERENCES . . . . .	63



## FIGURES

1.	Transformation for Boundary-Fitted Coordinate System . . .	18
2.	BFC Grid for JPL Nozzle . . . . .	24
3.	Mach Number Distribution at Wall and Centerline for JPL Nozzle (One-Phase Flow) . . . . .	24
4.	Mach Number Contour Plot for JPL Nozzle . . . . .	25
5.	Mach Number Distribution Throughout the Flow Field for JPL Nozzle . . . . .	25
6.	JPL Nozzle Throat Mach Number at Every Integration Step (Two-Phase Flow $W_j/W_m = 30\%$ ) . . . . .	27
7.	JPL Nozzle Mach Number Distribution at Wall and Centerline (Two-Phase Flow $W_j/W_m = 30\%$ ) . . . . .	28
8.	Velocity Lag (Two-Phase Flow $W_j/W_m = 30\%$ ) . . . . .	30
9.	Gas-to-Particle Temperature Ratio (Two-Phase Flow $W_j/W_m = 30\%$ ) . . . . .	31
10.	Particle Density Contour for $\bar{r}_j = 1\mu$ and $20\mu$ (Two-Phase Flow $W_j/W_m = 30\%$ ) . . . . .	32
11.	Particle Velocity Vector Plot for $\bar{r}_j = 1\mu$ and $20\mu$ (Two- Phase Flow $W_j/W_m = 30\%$ ) . . . . .	33
12.	JPL Nozzle Throat Mach Number at Every Integration Step (Two-Phase Flow $\bar{r}_j = 1\mu$ ) . . . . .	35
13.	JPL Nozzle Mach Number Distribution at Wall and Centerline (Two-Phase Flow $\bar{r}_j = 1\mu$ ) . . . . .	36
14.	Velocity Lag (Two-Phase Flow $\bar{r}_j = 1\mu$ ) . . . . .	38
15.	Gas-to-Particle Temperature Ratio (Two-Phase Flow $\bar{r}_j = 1\mu$ ) . . . . .	39
16.	Mach Number Contours for Different Particle Size (Two- Phase Flow $W_j/W_m = 30\%$ ) . . . . .	40

# FIGURES (Continued)

17.	Mach Number Contours for Different Particle Mass Fraction (Two-Phase Flow $\bar{r}_j = 1\mu$ ) . . . . .	40
18.	BFC Grid for Steep Entrance Nozzle . . . . .	42
19.	Mach Number Distribution at Wall and Centerline for Steep Entrance Nozzle . . . . .	43
20.	Throat Mach Number at Every Integration Step for Steep Entrance Nozzle . . . . .	43
21.	Mach Number Contour for Steep Entrance Nozzle . . . . .	44
22.	Mach Number Pictorial Plot for Steep Entrance Nozzle (One-Phase Flow) . . . . .	44
23.	Mach Number Pictorial Plot for Steep Entrance Nozzle (Two-Phase Flow) . . . . .	46
24.	Particle Density Contour for Steep Entrance Nozzle . . . . .	48
25.	Particle Density Pictorial Plot for Steep Entrance Nozzle . . . . .	48
26.	Pressure Distribution for Steep Entrance Nozzle . . . . .	49
27.	Velocity Lag and Temperature Ratio for Steep Entrance Nozzle . . . . .	49
28.	IUS Small Motor Interior Configuration and Computational Region . . . . .	52
29.	BFC Grid for Small IUS SRM with Submerged Nozzle Block . . . . .	52
30.	Blown-up BFC Grid in the Submerged and Throat Region for Small IUS SRM . . . . .	53
31.	Throat Mach Number at Every Integration Step for Small IUS SRM . . . . .	55
32.	Mach Number Distribution on the Boundary for Small IUS SRM Nozzle . . . . .	55

# FIGURES (Concluded)

33.	Mach Number Contour for Small IUS SRM (One-Phase Flow) . . . . .	56
34.	Velocity Vector Plot in the Submerged and Throat Region for Small IUS SRM (One-Phase Flow) . . . . .	56
35.	Gas-Phase Velocity Vector Plot in the Submerged and Throat Region for Small IUS SRM (Two-Phase Flow). . . . .	58
36.	Particle Velocity Vector Plot in the Submerged and Throat Region for Small IUS SRM (Two-Phase Flow) . . . . .	58
37.	Gas-Phase Mach Number Contour for Small IUS SRM (Two-Phase Flow) . . . . .	59
38.	Particle Density Contour for Small IUS SRM (Two-Phase Flow) . . . . .	59
39.	Velocity Lag and Temperature Ratio for Small IUS SRM . . .	59

## I. INTRODUCTION

The analysis of flow-through rocket motor exhaust nozzles has undergone continuous development for many years, since the optional design of these nozzles is dependent on accurate knowledge of the flow behavior and is important to the attainment of high thrust efficiencies for launch vehicles. The classic analytical solution technique based on the series expansion<sup>1, 2</sup> has limited application, as it requires the nozzle entrance to be suitably shaped. During the past decade the use of computers for the solution of nozzle flow fields<sup>3-8</sup> has been very popular among research engineers, mainly because the modern high-performance propulsion system, for the sake of length and weight reduction, usually possesses a nozzle contour with a small throat radius of curvature, a very steep wall gradient in the entrance region, or a submerged configuration, and the numerical technique is well-suited for application to different nozzle geometric configurations. For gas-only one-phase nozzle flows, various numerical methods used in the past were reviewed in Ref. 9.

<sup>1</sup>Hopkins, D.E. and D.E. Hill, "Effect of Small Radius of Curvature on Transonic Flow in Axisymmetric Nozzles," AIAA J., 4(8), Aug. 1966, p. 1337.

<sup>2</sup>Kliegel, J.R. and V. Quan, "Convergent-Divergent Nozzle Flows," AIAA J., Sept. 1968, p. 1728.

<sup>3</sup>Prozan, R.J., reported in "Numerical Solution of the Flowfield in the Throat Region of a Nozzle," by L.M. Saunders, BSVD-P-66TN-001 (NASA CR82601), Aug. 1966, Brown Engineering Co., Huntsville, Ala.

<sup>4</sup>Migdal, D., K. Klein, and G. Moretti, "Time-Dependent Calculations for Transonic Nozzle Flow," AIAA J., 7(1), Feb. 1969, p. 372.

<sup>5</sup>Wehofer, S. and W.C. Moger, "Transonic Flow in Conical Convergent and Convergent-Divergent Nozzles with Nonuniform Inlet Conditions," AIAA Paper No. 70-635.

<sup>6</sup>Laval, P., "Time-Dependent Calculation Method for Transonic Nozzle Flows," Lecture Notes in Physics, 8, Jan. 1971, p. 187.

<sup>7</sup>Serra, R.A., "Determination of Internal Gas Flows by a Transient Numerical Technique," AIAA J., 10(5), May 1972.

<sup>8</sup>Cline, M.C., "Computation of Steady Nozzle Flow by a Time-Dependent Method," AIAA J., 12(4), Apr. 1974, p. 419.

<sup>9</sup>Brown, E.F. and G.L. Hamilton, "A Survey of Methods for Exhaust-Nozzle Flow Analysis," AIAA Paper No. 60, 1975.

For the solid rocket motor, one of the prime causes of performance loss and surface damage is the presence of condensed metallic oxide particles of the combustion products in the flow field. The thermal and velocity lag associated with the particles often results in decreased nozzle efficiency and degradation of the motor's effectiveness in converting from thermal to kinetic energy. Hence, knowledge of the role played by the nongaseous combustion products in the rapid expansion through the throat region and the qualitative estimation of this influence are essential in the design of a thrust nozzle. A comprehensive review of investigations involving gas-particle nozzle flow fields before 1962 is presented in Ref. 10. More recent studies include the numerical iterative relaxation technique of Ref. 11 and an uncoupled flow model described in Ref. 12. While the analysis used in these studies is helpful in explaining some of the physical processes involved in the gas-particle flows in the transonic region, both suffer from the same weakness; i. e., the assumption that the gas-phase streamline coordinates are unaffected by the presence of particles. This assumption is particularly inappropriate for a nozzle with a very small throat radius of curvature or very steep wall gradient, since the presence of particles can alter the gas flow behavior. The constant fractional lag and the linear velocity profile assumptions used in Ref. 13 are not justified a priori. The results obtained or refined from a

---

<sup>10</sup>Hoglund, R. F., "Recent Advances in Gas-Particle Nozzle Flows," ARS Journal, May 1962, p. 662.

<sup>11</sup>Regan, J. F., H. D. Thompson, and R. F. Hoglund, "Two-Dimensional Analysis of Transonic Gas-Particle Flows in Axisymmetric Nozzles," J. Spacecraft, 8(4), Apr. 1971, p. 346.

<sup>12</sup>Jacques, L. J. and J. A. M. Seguin, "Two-Dimensional Transonic Two-Phase Flow in Axisymmetric Nozzles," AIAA Paper No. 74-1088, Oct. 1974.

<sup>13</sup>Kliegel, J. R. and G. R. Nickerson, "Axisymmetric Two-Phase Perfect Gas Performance Program," Report 02874-6006-R000, Vols. I and II, Apr. 1967, TRW Systems Group, Redondo Beach, Ca. 90278.

similar analysis for the transonic region<sup>14</sup> are highly uncertain, although they are the most widely used method in the propulsion industry. The one-dimensional analysis shown in Refs. 15 and 16, found useful in some areas, is not applicable to the study of a nozzle with a steep entrance.

In this report, the time-dependent method is applied to the solution of gas-only one-phase flow and fully coupled gas-particle two-phase flow inside nozzles of arbitrary geometry. The finite difference scheme and the inlet boundary conditions incorporated into the flow-field program are shown to yield good resolution of the entire subsonic-transonic-supersonic flow region. Moreover, to eliminate the computational difficulty associated with a nozzle with very steep wall or of a submerged configuration, the Boundary-Fitted-Coordinates (BFC) system<sup>17</sup> is adopted for generating a natural grid. Application of the BFC system to the nozzle flow study has greatly enhanced the capability of the flow-field program to solve problems which hitherto have not been extensively studied. The emphasis of the study has been placed on one- and two-phase flow in the transonic region. Various particle sizes and particle mass fractions have been investigated in the two-phase flow. The salient features associated with the two-phase nozzle flow compared with those of the one-phase flow are illustrated through calculations for a JPL nozzle configuration, for the Titan III solid rocket motor nozzle, and for the submerged nozzle configuration utilized in the IUS solid rocket motor.

<sup>14</sup>Coats, D. E., et al., "A Computer Program for the Prediction of Solid Propellant Rocket Motor Performance," Vols. I, II, and III, AFRPL-TR-75-36, July 1975.

<sup>15</sup>Soo, S. L., "Gas Dynamic Processes Involving Suspended Solids," A. I. Ch. E. Journal, 7(3), Sept. 1961, p. 384.

<sup>16</sup>Hultberg, J. A. and S. L. Soo, "Flow of a Gas-Solid Suspension Through a Nozzle," AIAA Paper No. 65-6, Jan. 1965.

<sup>17</sup>Thompson, J. F., F. C. Thames, and C. W. Martin, "Boundary-Fitted Curvilinear Coordinates Systems for Solution of Partial Differential Equations on Fields Containing Any Number of Arbitrary Two-Dimensional Bodies," NASA CR 2729, July 1977.

## II. GOVERNING EQUATIONS

The usual assumptions are employed below to derive the governing equations of a gas-particle two-phase flow.

- a. Mass conservation is applied to both mixture and individual phases.
- b. The mixture flow is adiabatic, i. e., the total energy of the mixture is constant.
- c. Gas phase is inviscid except for its interaction with the metallized particles, where the momentum exchange is considered for a viscous gas flow over spherical condensed particles.
- d. Energy exchange between the gas and particles occurs through both the convective and radiative heat transfer.
- e. The particles do not interact with each other, and the collision, condensation, and decomposition of the particles do not take place.
- f. The gas is a perfect gas and is chemically frozen.
- g. Volume occupied by the solid particle phase is negligible.

Based on the above assumptions and normalized by the gas-phase stagnation state corresponding to the condition at the inlet plane, the governing equations written in divergence form for an unsteady-state two-phase flow take the following form:

$$\frac{\partial \tilde{E}}{\partial t} + \frac{\partial \tilde{F}}{\partial x} + \frac{\partial \tilde{G}}{\partial r} + \tilde{H} = 0 \quad (1)$$

$$\begin{aligned}
\tilde{E} &= \begin{bmatrix} r^\delta \rho \\ r^\delta \rho u \\ r^\delta \rho v \\ r^\delta e \\ r^\delta \rho_j (N-1) \\ r^\delta \rho_j u_j (N-1) \\ r^\delta \rho_j v_j (N-1) \\ r^\delta h_j (N-1) \end{bmatrix}, & \tilde{F} &= \begin{bmatrix} r^\delta \rho u \\ r^\delta (\tau p + \rho u^2) \\ r^\delta \rho_{uv} \\ r^\delta [e + (\gamma-1)p]u \\ r^\delta \rho_j u_j (N-1) \\ r^\delta \rho_j u_j^2 (N-1) \\ r^\delta \rho_j u_j v_j (N-1) \\ r^\delta h_{j,u_j} (N-1) \end{bmatrix} \\
\tilde{G} &= \begin{bmatrix} r^\delta \rho v \\ r^\delta \rho_{uv} \\ r^\delta (\tau p + \rho v^2) \\ r^\delta [e + (\gamma-1)p]v \\ r^\delta \rho_j v_j (N-1) \\ r^\delta \rho_j u_j v_j (N-1) \\ r^\delta \rho_j v_j^2 (N-1) \\ r^\delta h_{j,v_j} (N-1) \end{bmatrix}, & \tilde{H} &= \begin{bmatrix} 0 \\ r^\delta \rho_{j,A_j} (u-u_j) (N-1) \\ r^\delta \rho_{j,A_j} (v-v_j) (N-1) - \delta \tau p \\ r^\delta \rho_{j,A_j B_j} (N-1) \\ 0 \\ -r^\delta \rho_{j,A_j} (u-u_j) (N-1) \\ -r^\delta \rho_{j,A_j} (v-v_j) (N-1) \\ -r^\delta \rho_{j,A_j B_j} (N-1) \end{bmatrix}
\end{aligned}$$



where

$$\begin{cases} N = 1 & \text{one-phase gas-only} \\ N = 2 & \text{two-phase flow} \end{cases}$$

$$\begin{cases} \delta = 0 & \text{two-dimension} \\ \delta = 1 & \text{axisymmetry} \end{cases}$$

The nondimensional parameters used here are gas-phase stagnation pressure  $\bar{p}_{t1}$ , stagnation density  $\bar{\rho}_{t1}$ , stagnation energy per unit volume  $\bar{e}_{t1} = \bar{p}_{t1}/(\gamma-1)$ , maximum speed  $\bar{V}_{max1}$ , and stagnation temperature  $\bar{T}_{t1}$  evaluated at the inlet plane, so that

$$p = \bar{p}/\bar{p}_{t1}, \quad \tau = (\gamma-1)/2\gamma, \quad t = \bar{V}_{max1} \bar{t}/\bar{L}$$

$$\rho = \bar{\rho}/\bar{\rho}_{t1}, \quad \rho_j = \bar{\rho}_j/\bar{\rho}_{t1}, \quad x = \bar{x}/\bar{L}$$

$$u = \bar{u}/\bar{V}_{max1}, \quad u_j = \bar{u}_j/\bar{V}_{max1}, \quad r = \bar{r}/\bar{L}$$

$$v = \bar{v}/\bar{V}_{max1}, \quad v_j = \bar{v}_j/\bar{V}_{max1}, \quad \text{for } \bar{L} = \text{reference length scale (e.g., unit foot)}$$

$$e = \bar{e}/\bar{e}_{t1}, \quad h_j = \bar{h}_j/\bar{e}_{t1}$$

where  $\bar{\rho}, \bar{u}, \bar{v}, \bar{p}$ , and  $\bar{e}$  are the dimensioned density, horizontal x-component velocity, vertical r-component velocity, pressure, and energy per unit volume, respectively, for the gas phase; and  $\bar{\rho}_j, \bar{u}_j, \bar{v}_j$ , and  $\bar{h}_j$  are the dimensioned density, x-component velocity, r-component velocity, and energy per unit volume, respectively, for the particle phase. There are also

Friction term:

$$A_j = \frac{9}{2} \frac{\bar{\mu}_{g,j} f_j}{\bar{m}_j \bar{r}_j^2} \frac{\bar{L}}{\bar{V}_{max1}}$$

Energy exchange term:

$$B_j = 2\gamma[q_j \cdot \Delta q_j - g_c(T_j - T) - g_r(\epsilon_j T_j^4 - \epsilon T^4)]$$

where

$$g_c = N_{uj}/6 f_j P_r, \quad g_r = \bar{\sigma} \bar{r}_j T_{t1}^3 / 3 \bar{c}_p \bar{\mu}_g f_j$$

$$q_j \cdot \Delta q_j = u_j(u - u_j) + v_j(v - v_j)$$

$$T_j = \bar{T}_j / \bar{T}_{t1} = [h_j / \gamma \rho_j - (u_j^2 + v_j^2)] / \omega$$

$$T = \bar{T} / \bar{T}_{t1} = p / \rho, \quad \omega = \bar{c}_j / \bar{c}_p$$

with

$\bar{t}$  = dimensioned time

$\bar{T}$  = dimensioned gas temperature

$\bar{\mu}_g$  = gas viscosity

$\bar{T}_j$  = dimensioned particle temperature

$\bar{m}_j$  = particle mass density

$\bar{r}_j$  = particle radius

$\bar{c}_p$  = gas specific heat at constant pressure

$\bar{c}_j$  = particle heat capacity

$\gamma$  = gas specific heat ratio

$\bar{\sigma}$  = Stefan-Boltzmann constant

$\epsilon_j$  = particle emissivity

$\epsilon$  = gas emissivity

$\bar{r}$  = dimensioned radial coordinate

$P_r$  = gas Prandtl number

$\bar{x}$  = dimensioned axial coordinate

The momentum transfer parameter  $f_j$  is defined as

$$f_j = C_D / C_{D_{\text{Stokes}}}$$

where  $C_D$  is the drag coefficient based on C. B. Henderson's correlation equation<sup>18</sup> for spheres in continuum and rarefied flows, and  $C_{D_{\text{Stokes}}} = Re_j/24$  is the Stokes law of drag coefficient for spheres in creeping motion.

The heat transfer parameter, particle Nusselt number, is taken as

$$N_{uj} = 2 + 0.459 Re_j^{0.55} P_r^{0.33}$$

The particle Reynolds number is based on the relative speed  $|\Delta \bar{q}_j| = |\Delta \bar{q}_j| / \bar{v}_{\text{max}1} = \sqrt{(u-u_j)^2 + (v-v_j)^2}$  and the particle radius  $\bar{r}_j$ , and is defined as follows:

$$Re_j = \frac{2 |\Delta \bar{q}_j| \bar{r}_j \bar{\rho}}{\bar{\mu}_g} = 2 |\Delta \bar{q}_j| \bar{\rho} \frac{\bar{r}_j}{\bar{\mu}_g} \frac{1}{\bar{\tau}} \frac{\bar{p}_{t1}}{\bar{v}_{\text{max}1}}$$

The gas viscosity is evaluated from

$$\bar{\mu}_g = \bar{\mu}_{t1} \left( \frac{\bar{T}}{\bar{T}_{t1}} \right)^A = \bar{\mu}_{t1} \left( \frac{P}{\bar{\rho}} \right)^A$$

where  $\bar{\mu}_{t1}$  is the gas viscosity at the stagnation temperature  $\bar{T}_{t1}$  corresponding to the inlet condition, and A is an input constant.

<sup>18</sup>Henderson, C. B., "Drag Coefficients of Spheres in Continuum and Rarefied Flows," AIAA J., 14(6), June 1976, p. 707.

It is often debated which form of the equation the drag coefficient  $C_D$  and the particle Nusselt number  $Nu_j$  should take. The correlating equations of Ref. 18 provide accurate representations of sphere drag coefficients over a wide range of flow conditions. The simple form of the particle Nusselt number is adopted from Ref. 19. If more advanced parametric equations are available, they can be incorporated easily into the present analysis without much modification.

The computer program Dusty Transonic Internal Flows (DTIF) has been developed so that, for the gas-only one-phase flow ( $N=1$ ), all the particle phase calculations are bypassed.

---

<sup>19</sup>Carlson, D.J. and R. F. Hoglund, "Particle Drag and Heat Transfer in Rocket Nozzles," AIAA J., 2(11), 1964, p. 1980.

### III. NUMERICAL ASPECTS

From a general arbitrary nozzle configuration in the physical plane  $x, r$  the transformation to a grid with uniform square mesh in the computational plane  $\zeta, \xi$  can be accomplished by using BFC; this requires the solution of two elliptical partial differential equations with Dirichlet boundary conditions.<sup>17</sup> Figure 1 illustrates the transformation relationship. The solution utilizing the successive over-relaxation (SOR) method for generating the boundary-fitted coordinates is carried out by the TOMCAT program, and the scale factors for transformation are computed in the FATCAT program.<sup>17</sup>

Formally applying the chain rule of change of independent variables for Eq. (1) results in the following conservation laws in the  $\zeta, \xi$  plane:

$$\frac{\partial E}{\partial t} + \frac{\partial F}{\partial \zeta} + \frac{\partial G}{\partial \xi} + H = 0 \quad (2)$$

where

$$\begin{cases} E = \tilde{E}J_2 \\ F = \tilde{F}r_\xi - \tilde{G}x_\xi \\ G = \tilde{F}r_\zeta + \tilde{G}x_\zeta \\ H = \tilde{H}J_2 \end{cases}$$

and  $J_2 = x_\zeta r_\xi - x_\xi r_\zeta$  is the Jacobian of transformation. For a particular nozzle geometry and transformation, the Jacobian and the partial derivatives are computed in the FATCAT\* program and stored on disk for flow field study.

---

\*For a simple region such as the nozzle geometry considered herein, the FATCAT program gives the values of scale factors at the corner points twice as large as they should be. This has been corrected for the nozzle application in this study.

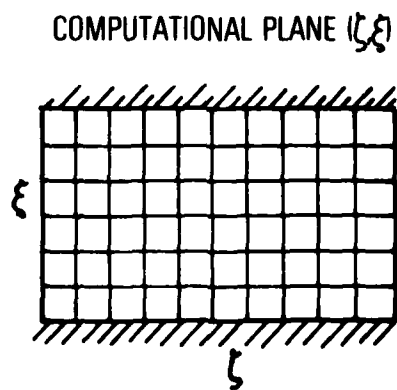
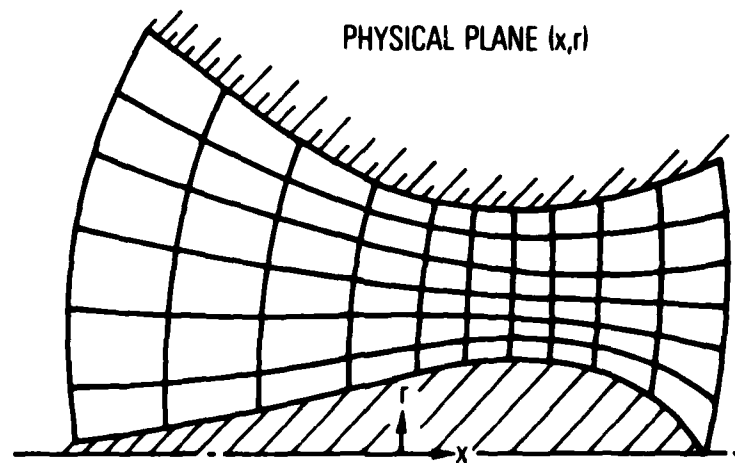


Fig. 1. Transformation for Boundary-Fitted Coordinate System

Through insertion of the unsteady term in the governing Eq. (1), the differential equation is cast into hyperbolic type; therefore, the complication associated with the mixed flow phenomenon necessarily existing in a steady-state analysis is eliminated. The MacCormack finite difference scheme<sup>20</sup> which has been applied successfully to nozzle flow problems<sup>21</sup> is adopted here for the solution of the partial differential Eq. (2).

For one-phase flow, the initial condition is based on a one-dimensional isentropic analysis with the flow vector set to the local inclination angle from linear interpolation between the lower and upper wall slopes along the same grid line (constant  $\zeta$ ). The converged one-phase results serve, then, as the initial guess for the gas-phase data in the two-phase flow.

For the particle-phase arrays of initial velocity lags  $\lambda_v$  and temperature ratios  $\lambda_T$  are chosen, and the initial condition (guess) is

$$\begin{aligned}\rho_j &= \rho \phi / (1 - \phi), & u_j &= u \lambda_v, & v_j &= v \lambda_v \\ T_j &= T / \lambda_T, & h_j &= \gamma \rho_j [\omega T_j + (u_j^2 + v_j^2)]\end{aligned}$$

where  $\phi = W_j / W_m$  is the particle mass fraction and  $\omega = \bar{C}_j / \bar{C}_p$  is the ratio of particle heat capacity to gas specific heat at constant pressure.

A unit velocity lag and temperature ratio as an initial guess of particle phase are satisfactory for this study.

The initial guess based on the so-called Equilibrium Gas-Particle Mixture (EGPM), which is itself a physically meaningless term with its isentropic index derived from

$$\gamma_m = \gamma \frac{1 + \omega \phi (1 - \phi)}{1 + \gamma \omega \phi (1 - \phi)}$$

is not appropriate for the fully coupled two-phase flow study.

<sup>20</sup> MacCormack, R. W., "The Effect of Viscosity in Hypervelocity Impact Cratering," AIAA Paper 69-354, May 1969.

<sup>21</sup> Chang, I-Shih, "Three-Dimensional Supersonic Internal Flows," AIAA Paper 76-423, July 1976.

The exit boundary condition is based on a simple linear extrapolation since the mixture flow is assumed to be supersonic at the exit plane, and the error generated from the extrapolation is not expected to propagate back and affect the upstream results.

The inlet boundary condition for horizontal inflow is computed from a characteristics formulation similar to that of Ref. 7, which provides fairly smooth subsonic flow in the physical domain. For radial inflow, e.g., the IUS motor studied herein, the experimentally evaluated propellant burning rate and chamber pressure/temperature data supply needed information at the propellant burning surface, and a linear interpolation for smoothing flow variables at the grid line adjacent to the propellant burning surface is required to avoid instability in the inlet region.

For a nozzle with a centerbody, the flow variables at the boundary are obtained from linear extrapolation of the data from two adjacent interior points and then modified by the local tangency condition. Without the centerbody in the axisymmetric nozzle, the flow variables take undetermined form at the centerline. The standard L'Hospital's rule with the symmetry consideration is used to evaluate all the physical flow variables except the radial velocity, which is zero at the singular centerline. Also, if notice is taken that all the conservative variables at the centerline are zero except  $H_3 = -\tau p$  (i.e., no restriction is imposed on the gas pressure change at the centerline), a smoothing process involving a linear interpolation for resetting the gas-phase radial velocity  $v$  at the first interior point above the centerline is found helpful in stabilizing the solution.

It is important also to retain the fourth-order damping terms to the second-order MacCormack finite difference scheme for the unsteady state application in order to eliminate the nonlinear instability. The formulation adopted here is similar to that of Ref. 22 with a damping coefficient equal to 0.01.

---

<sup>22</sup> Kutler, P., L. Sakell, and G. Aiello, "On the Shock-on-Shock Interaction Problem," AIAA Paper No. 74-524, June 1974.



The integration step size is governed by the local CFL condition similar to that used in Ref. 5 and determined by the following expressions:

$$\Delta t = \min \frac{\Delta l}{q + a}$$

where

$$\Delta l = \sqrt{(\Delta x)^2 + (\Delta r)^2}, \quad q = \sqrt{u^2 + v^2}$$

and  $a = \sqrt{T(\gamma-1)/2}$  is the dimensionless local sonic speed.

#### IV. NOZZLE WITH SMALL THROAT RADIUS OF CURVATURE--JPL NOZZLE

##### A. ONE-PHASE FLOW

The compressible flow inside the JPL axisymmetric nozzle<sup>23</sup> with 45° entrance and 15° exit straight wall tangent to a circular throat (with ratio of throat radius of curvature to throat height = 0.625) provides a classic comparison for the present nozzle flow study. Figure 2 shows the physical grid generated from the boundary-fitted coordinates system mentioned above. The computed Mach number distributions along the wall and along the centerline are illustrated in Fig. 3; the test data are also shown for comparison. Figure 4 is the Mach number contour plot, and Fig. 5 shows the Mach number at all the grid points in the physical plane. The theoretical gas-only one-phase result from this study agrees very well with the test data in the entire subsonic-transonic-supersonic flow region. This can be attributed to the good resolution of the boundary flow variables through the use of boundary-aligned grid arrangement. Note the smoothness of the Mach number distribution in the subsonic region computed by the present method. The recompression waves in the supersonic region, which necessarily occur due to over-expansion of the flow near the wall downstream of the throat with small radius of curvature, eventually coalesce into a shock wave near the centerline in the far-downstream region. This flow behavior has been observed in the test<sup>7</sup> and is visible from Figs. 4 and 5.

The convergence criterion used in all the calculations shown herein requires that the difference in Mach number is at least 0.01% and in the mass flow rate is 0.001% at the throat for three consecutive time integration steps. For the JPL nozzle with 61 x 31 grid points, the converged solution requires 623 integration steps and takes 6 min, 17 sec execution time on the CDC 7600 computer. The theoretical results agree well with the test data for this

<sup>23</sup>Cuffel, R. F., L. H. Back, and P. F. Massier, "Transonic Flowfield in a Supersonic Nozzle with Small Throat Radius of Curvature," AIAA J., 7(7), July 1969, p. 1364.

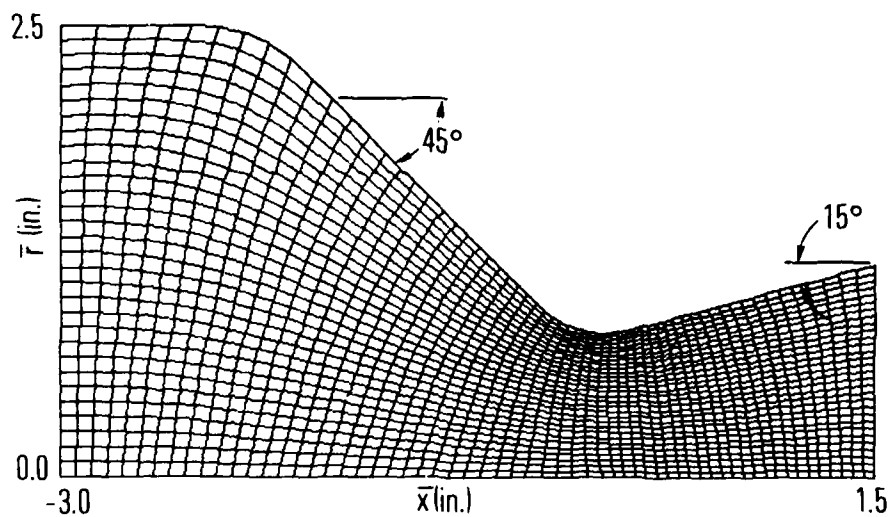


Fig. 2. BFC Grid for JPL Nozzle

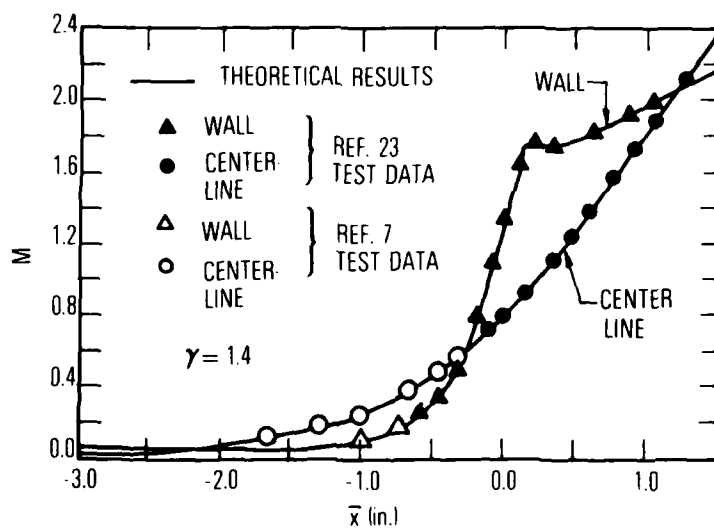


Fig. 3. Mach Number Distribution at Wall and Centerline for JPL Nozzle (One-Phase Flow)

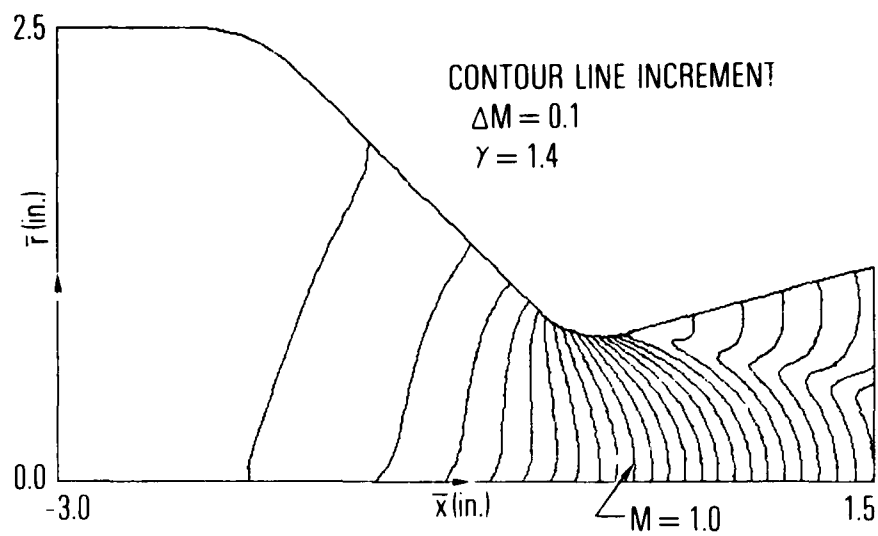


Fig. 4. Mach Number Contour Plot for JPL Nozzle

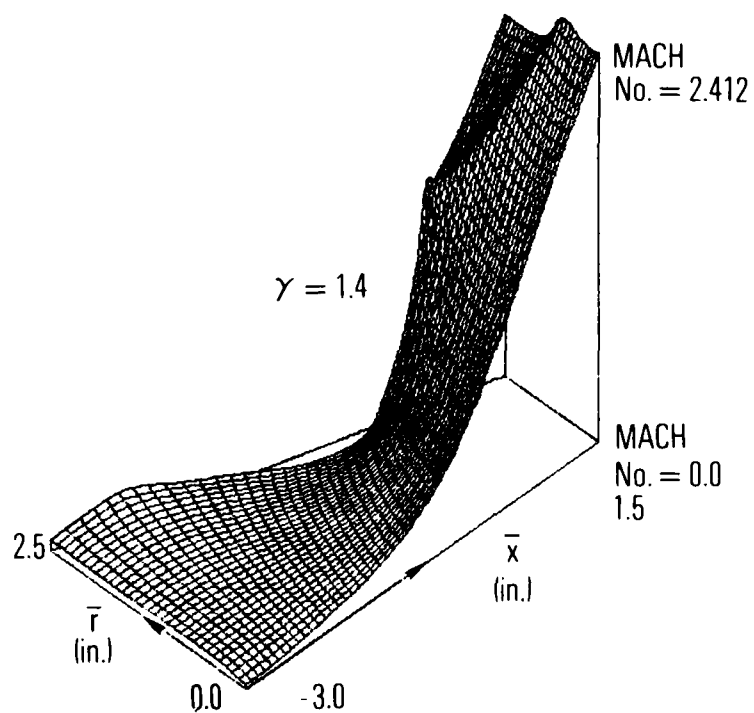


Fig. 5. Mach Number Distribution Throughout the Flow Field for JPL Nozzle

nozzle study, thus assuring further application of the computer code to other nozzle configurations.

## B. TWO-PHASE FLOW

The same flow field program is applied to the fully-coupled gas-particle two-phase nozzle flow with the two-phase index  $N$  in Eq. (1) set to 2. For the two-phase flow calculation, the following data are adopted.

<u>Gas Phase (Air)</u>	<u>Particle Phase</u>
$\bar{C}_p = 0.255 \text{ Btu/lb}_m\text{-}^\circ\text{R}$	$\bar{C}_j = 0.33 \text{ Btu/lb}_m\text{-}^\circ\text{R}$
$\bar{\mu}_{t1} = 1.8 \times 10^{-5} \text{ lb}_m/\text{ft-sec}$	$\bar{m}_j = 250 \text{ lb}_m/\text{ft}^3$
$\gamma = 1.4, \text{ Pr} = 0.74$	
$A = 0.6$	

The chamber condition is taken to be  $\bar{T}_{t1} = 1000^\circ\text{R}$ ,  $\bar{P}_{t1} = 150 \text{ psia}$ . Also,  $\epsilon_j = 0.1$  and  $\epsilon = 0.05$  are used for the radiative heat exchange between the gas and spherical particles.

The previously computed one-phase flow result is taken as the initial guess for the two-phase flow. Different particle sizes and particle mass fractions  $W_j/W_m$  are calculated. Figure 6 shows the variation of the computed throat Mach number along the wall and along the centerline at each timewise integration step (iteration) for various particle sizes at the same  $W_j/W_m = 30\%$ . At 300 iterations the two-phase transonic flow region is essentially established. Further integration does not produce appreciable change in the throat flow field, as is evidenced from the continued calculation with  $\bar{r}_j = 1\mu$  to 600 integration steps. Figure 7 shows the computed wall and centerline gas phase Mach number distribution for various particle sizes with the same  $W_j/W_m = 30\%$ . For comparison, the previously computed

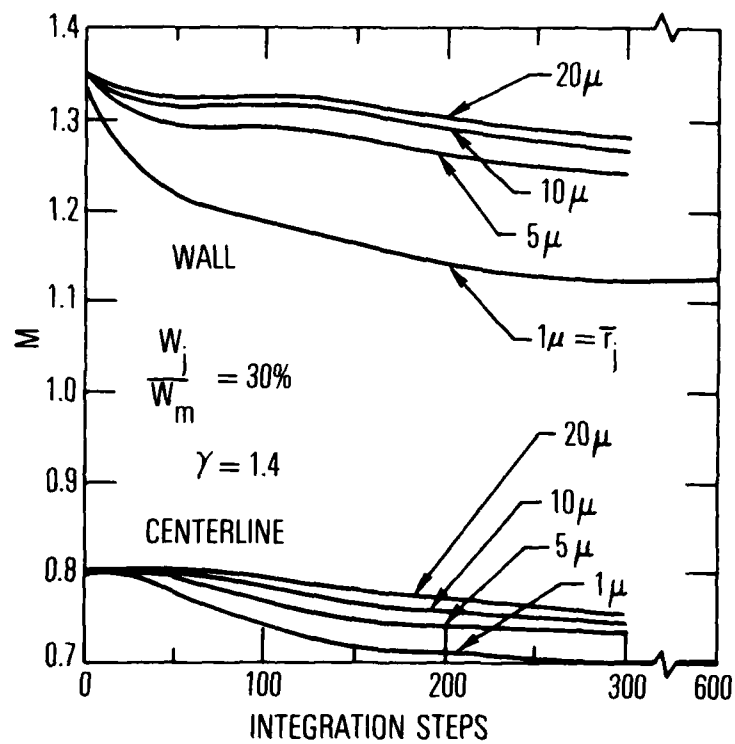


Fig. 6. JPL Nozzle Throat Mach Number at Every Integration Step (Two-Phase Flow  $\frac{W_j}{W_m} = 30\%$ )

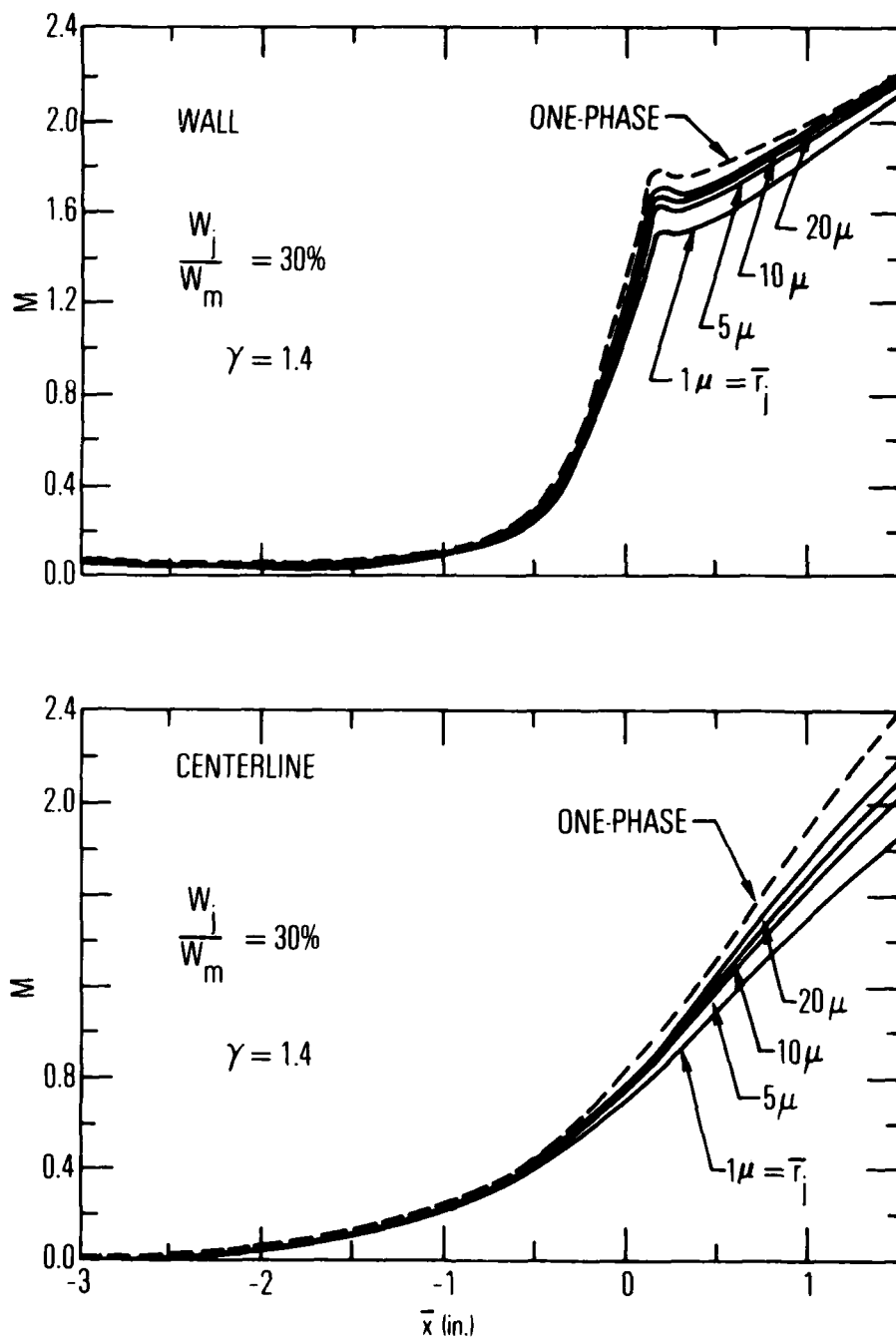


Fig. 7. JPL Nozzle Mach Number Distribution at Wall and Centerline (Two-Phase Flow  $W_j/W_m = 30\%$ )

gas-only one-phase results are plotted as dashed curves. Some of the features associated with the fully-coupled two-phase nozzle flow in comparison with that of gas-only one-phase flow are found in Figs. 6 and 7. While lower gas speed is observed both on the wall and centerline in the two-phase flow field than that in the gas-only one-phase, the small-sized particles act more effectively to slow down the gas-phase expansion than that of large-sized particles for the same particle mass fraction. This is physically correct, since for the same particle mass fraction the total particle surface area effective for momentum and energy exchange between gas and particles is greater in a two-phase flow field involving smaller diameter particles. Figure 8 gives the velocity lag  $q_j/q$  at the throat and at the exit plane, respectively, and Fig. 9 shows the results for the temperature ratio  $T/T_j$ . The temperature ratio defined here illustrates the thermal lag between the particle and gas and is less sensitive to the small variation in the computed numerics than the commonly used thermal lag  $(1-T_j)/(1-T)$ , especially in the low subsonic region when both gas and particle temperatures are very close to the reference gas stagnation temperature at the inlet plane. The large particle in the two-phase flow field lags much more behind the gas phase flow and exhibits a wider region of particle free zone than that of the small particle. Moreover, in comparison with the present fully coupled two-phase analysis, the constant fractional lag assumption used in Ref. 13 is justified only for a two-phase flow with high loading ratio of very small particles.

The effect of different particle sizes in the two-phase flow can be visualized best by comparison of the calculated particle density contour and particle-phase velocity vector plot for the small ( $\bar{r}_j = 1\mu$ ) and the large ( $\bar{r}_j = 20\mu$ ) particles depicted in Figs. 10 and 11. These figures show that for the flow with  $1\mu$  radius particles a sharp change in particle density is obtained near the upper wall downstream of the throat, and the particle density drastically decreases to a small value. But it does not vanish exactly at the wall. With the large ( $\bar{r}_j = 20\mu$ ) particle flow, however, a very distinctive



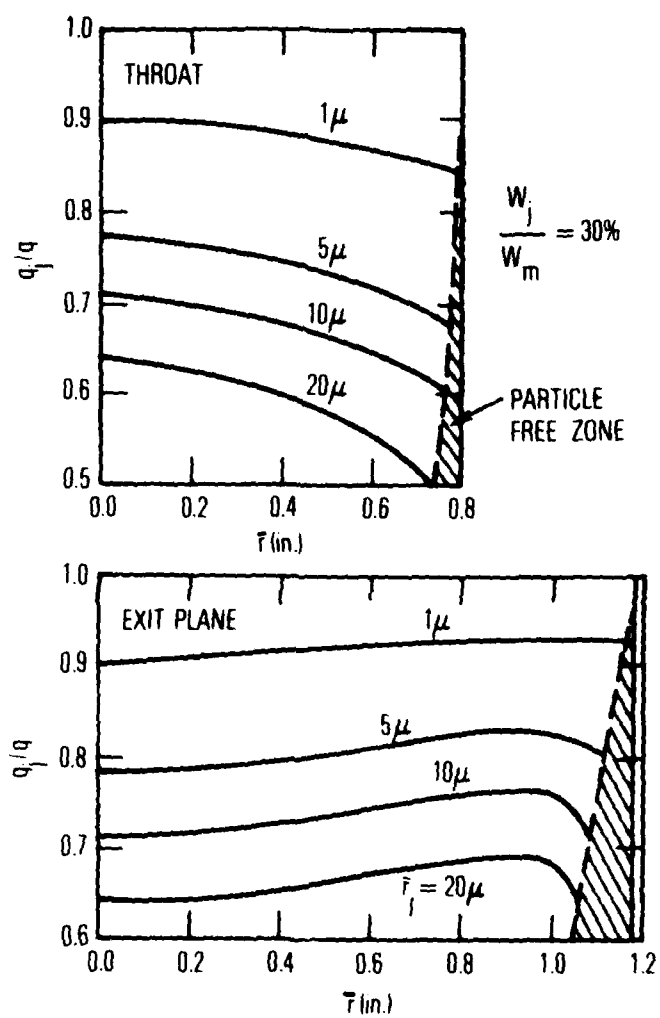


Fig. 8. Velocity Lag (Two-Phase Flow  $W_j/W_m = 30\%$ )

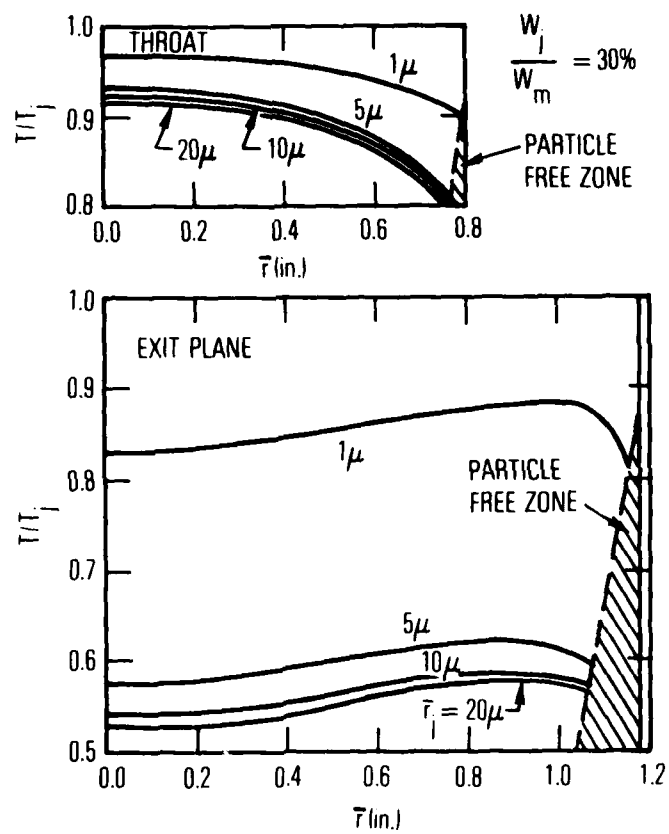


Fig. 9. Gas-to-Particle Temperature Ratio  
 (Two-Phase Flow  $W_j/W_m = 30\%$ )

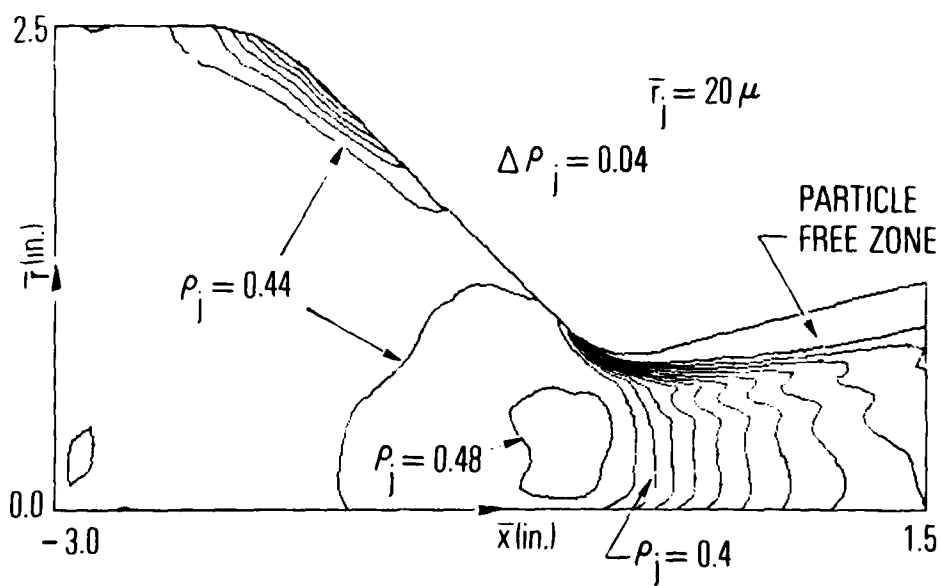
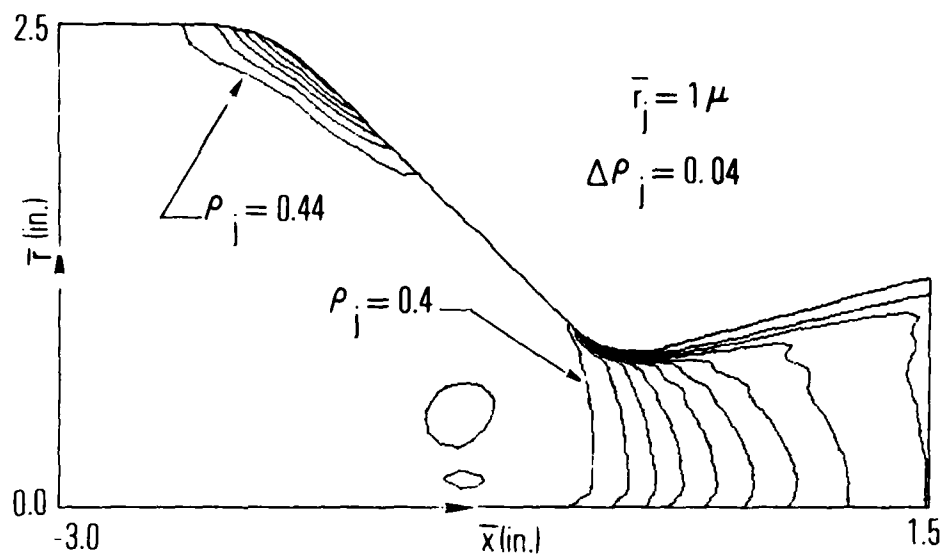


Fig. 10. Particle Density Contour for  $\bar{r}_j = 1\mu$  and  $20\mu$   
(Two-Phase Flow  $W_j/W_m = 30\%$ )

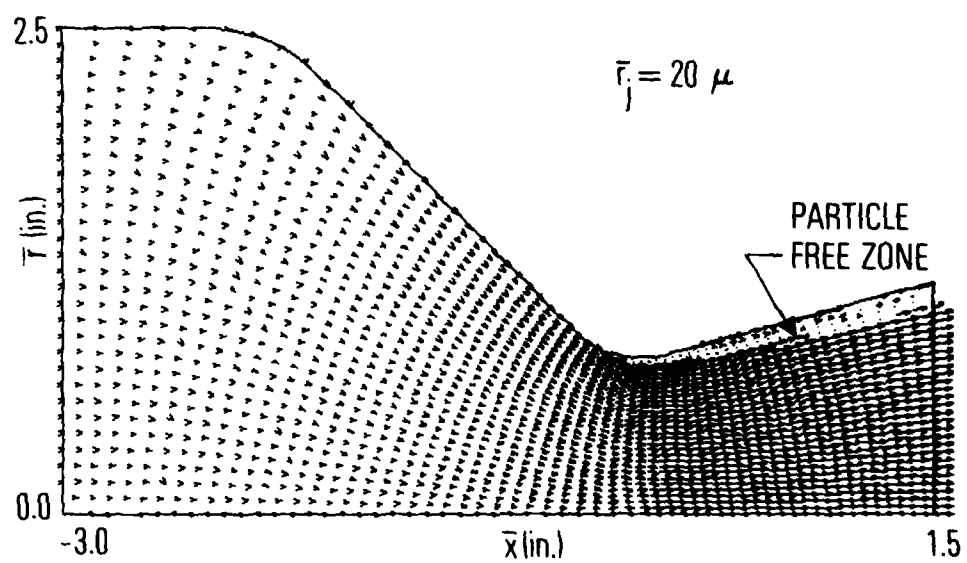
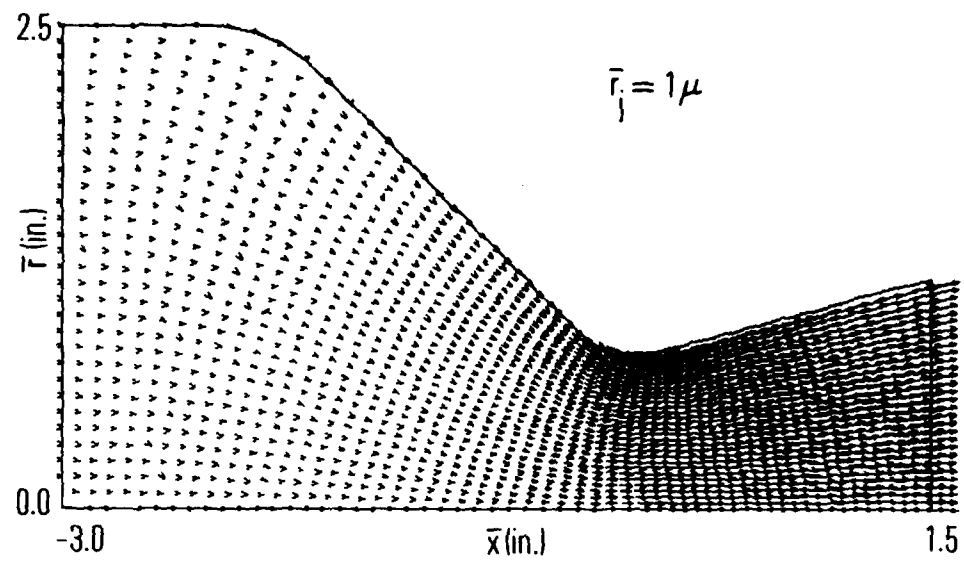


Fig. 11. Particle Velocity Vector Plot for  $\bar{r}_j = 1\mu$  and  $20\mu$   
(Two-Phase Flow  $W_j/W_m = 30\%$ )

particle-free zone appears in the calculated result and can be seen from either Fig. 10 or Fig. 11. Since the heavier particles apparently cannot effectively turn around the throat corner with small throat radius of curvature and evidently tend to cluster near the centerline, there are essentially no particles present near the wall downstream of the throat to slow down the gas expansion. This explains why, in Fig. 7, the difference between the Mach numbers in one-phase and in large particle two-phase flows near the nozzle lip region is virtually nil, but not so at the exit centerline region.

The variation of the computed throat gas phase Mach number along the wall and along the centerline at each timewise integration step for a different particle mass fraction  $W_j/W_m$  at a given particle radius  $\bar{r}_j = 1\mu$  is indicated in Fig. 12. Figure 13 shows the corresponding wall and centerline gas phase Mach number distribution. As before, the dashed curves are the results for the gas-only one-phase flow. It is obvious from these figures that a reduction of particle mass fraction immediately reduces the two-phase "drag" effect. A high particle mass fraction ( $W_j/W_m \geq 45\%$ ) produces an entirely subsonic flow at the geometric throat for the nozzle geometry considered. It is then possible to adjust the exit Mach number from supersonic all the way down to subsonic by varying the particle mass fraction and/or the particle size. The lip shock extending to the exhaust plume field which occurs in the over- and under-expanded case<sup>24,25</sup> could also be weakened or eliminated through the particle drag effect.

A close look at Figs. 6 and 12 also reveals the fact that care must be taken in the case of large particle mass fraction flows ( $W_j/W_m > 45\%$ ) and very small-sized particle flows ( $\bar{r}_j < 0.5\mu$ ) in starting from the one-phase initial guess. A sharp drop in the wall Mach number at or near downstream

<sup>24</sup>Chow, W. L. and I-Shih Chang, "Mach Reflection Associated with Over-expanded Nozzle Free Jet Flows," AIAA J., 13(6), June 1975.

<sup>25</sup>Chang, I-Shih and W. L. Chow, "Mach Disc from Underexpanded Axisymmetric Nozzle Flow," AIAA J., 12, Aug. 1974, p. 1079.

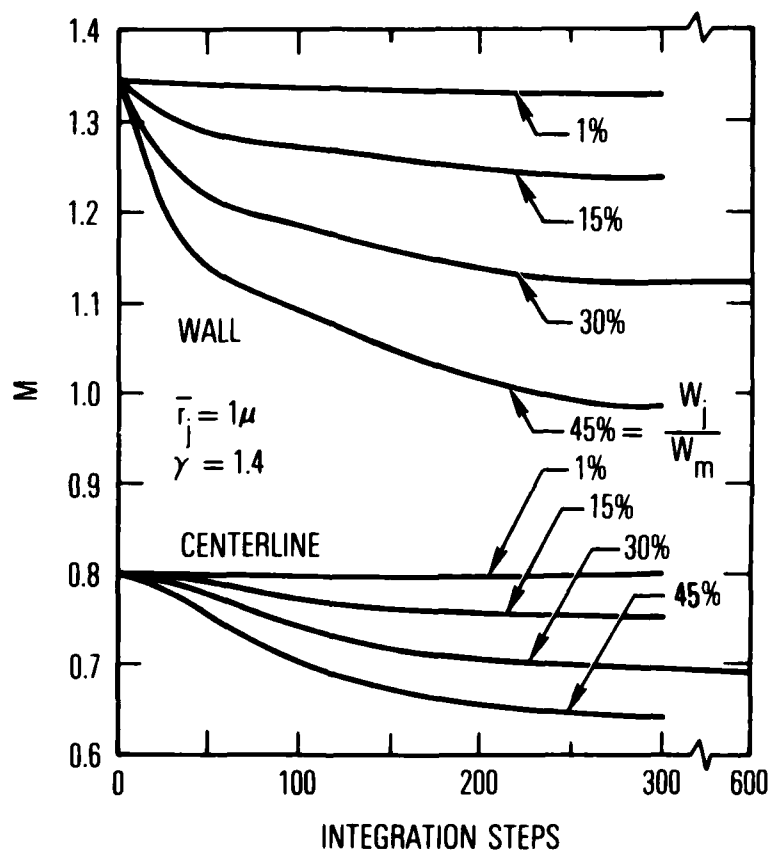


Fig. 12. JPL Nozzle Throat Mach Number at Every Integration Step (Two-Phase Flow  $\bar{r}_j = 1\mu$ )

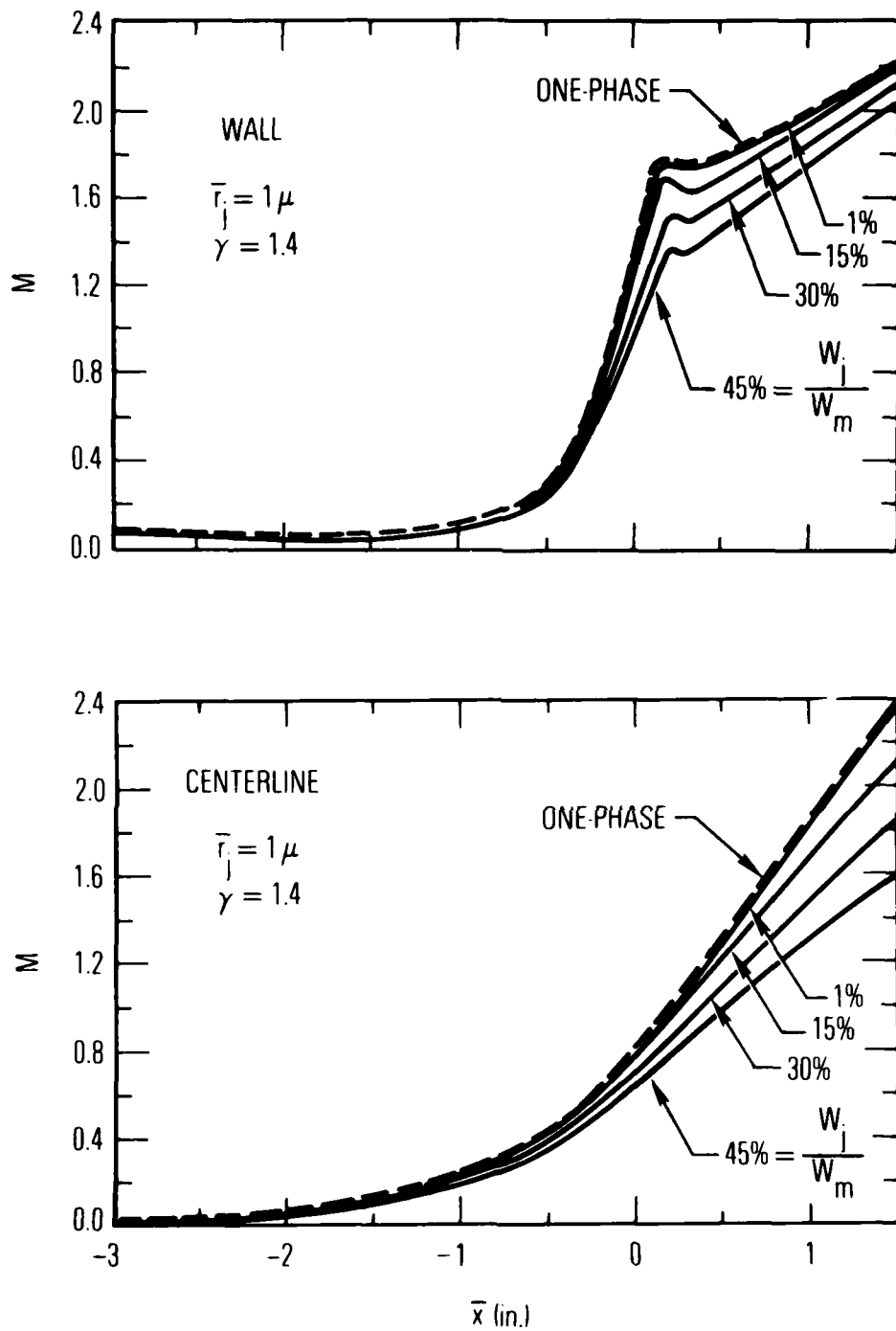


Fig. 13. JPL Nozzle Mach Number Distribution at Wall and Centerline (Two-Phase Flow  $\bar{r}_j = 1\mu$ )

of the throat can be expected, especially when the throat radius of curvature is small, necessitating the use of small time marching step at the beginning of the two-phase calculation. Furthermore, the possibility of subsonic flow occurring at the exit plane requires modification of the supersonic downstream boundary condition or the extension of the exit boundary to a farther downstream location.

Figures 14 and 15 show the computed velocity lag and temperature ratio for various particle mass fractions at a fixed  $\bar{r}_j = 1\mu$ . Figure 16 summarizes several Mach number contours,  $M = 0.1, 0.2, 0.5, 1.0$ , and  $1.5$ , for various particle sizes at a fixed ratio  $W_j/W_m = 30\%$ , and Fig. 17 is the similar result for various particle mass flow ratios at a fixed radius  $\bar{r}_j = 1\mu$ . As before, the dashed curves are the results for a gas-only one-phase flow. A typical two-phase run involving 300 integration steps takes approximately 7 min execution time on the CDC 7600 computer.



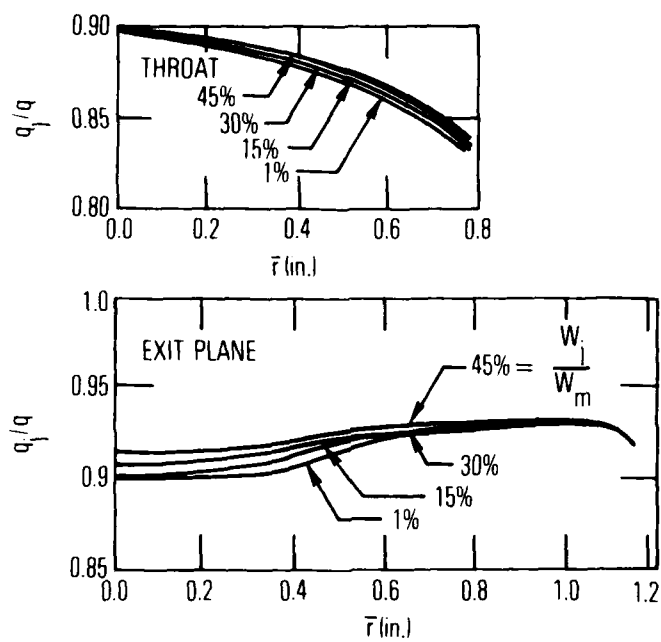


Fig. 14. Velocity Lag (Two-Phase Flow  $\bar{r}_j = 1\mu$ )

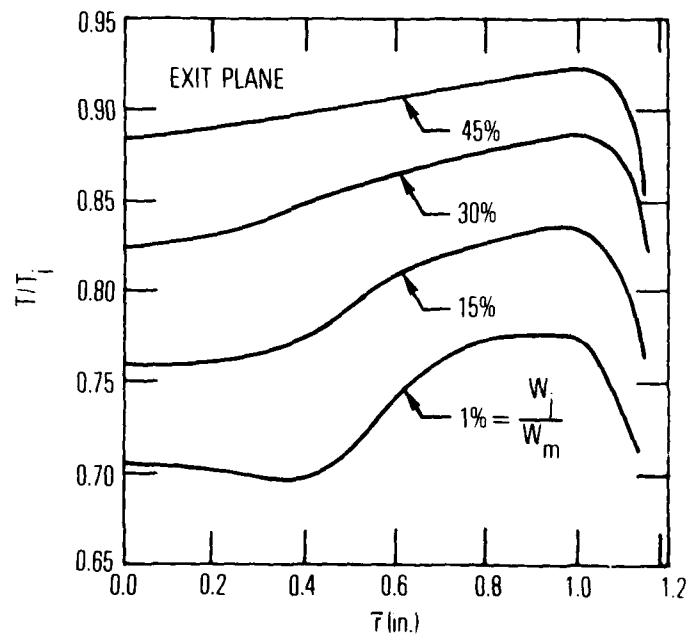
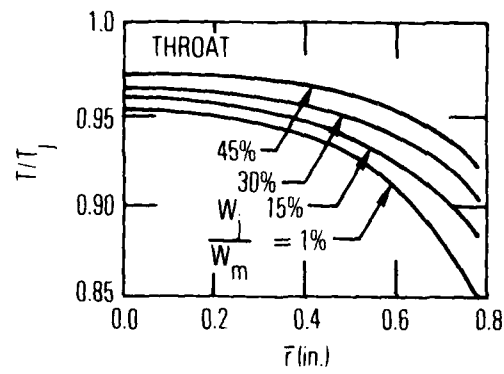


Fig. 15. Gas-to-Particle Temperature Ratio  
(Two-Phase Flow  $\bar{r}_j = 1\mu$ )

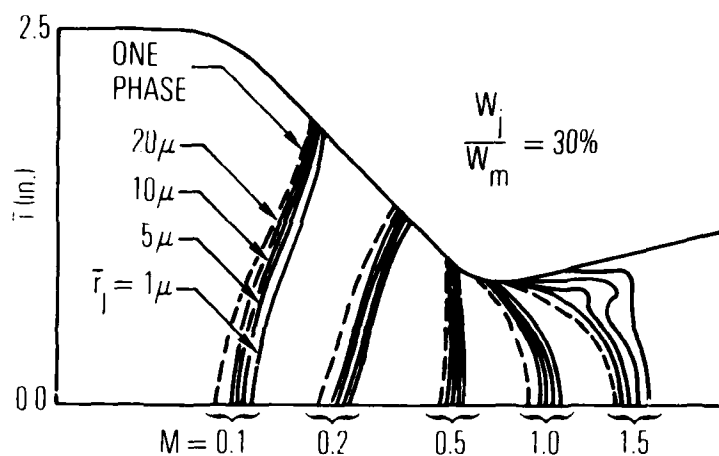


Fig. 16. Mach Number Contours for Different Particle Size  
(Two-Phase Flow  $W_j/W_m = 30\%$ )

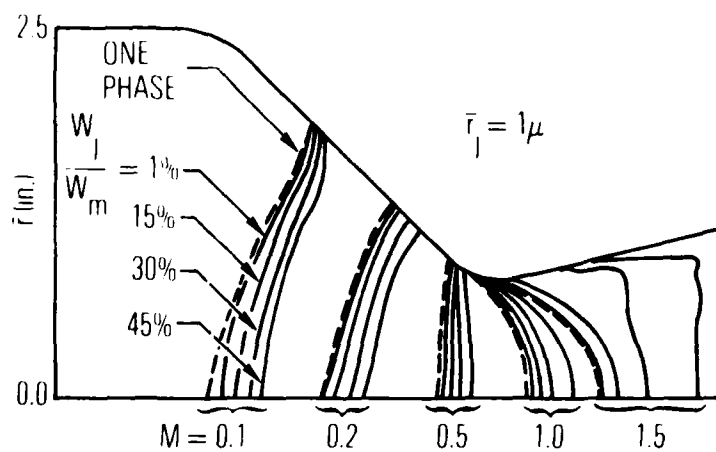


Fig. 17. Mach Number Contours for Different Particle Mass  
Fraction (Two-Phase Flow  $\bar{r}_j = 1\mu$ )

## V. NOZZLE WITH VERY STEEP ENTRANCE--TITAN III MOTOR

### A. ONE-PHASE FLOW

A severe test of the present numerical technique is the solution of the compressible flow field inside a nozzle with near vertical entrance region shown in Fig. 18, which also illustrates the grid generated from the boundary-fitted coordinates system. The nozzle steep entrance contour is that of the Titan III solid rocket motor nozzle.<sup>26</sup> The specific heat for the combustion products is  $\gamma = 1.19$ . The computed wall and centerline Mach number distribution is given in Fig. 19. The same nozzle was analyzed with  $\gamma = 1.4$ , and the results are also plotted on the same figure which serves to illustrate the effect of different  $\gamma$  on the Mach number distribution. Figure 20 depicts the computed throat Mach number at every integration step. The converged one-phase flow solution for  $\gamma = 1.19$  requires 890 integration steps and takes 8 min, 58 sec on the CDC 7600 computer. Figure 21 is the Mach number contour plot, and Fig. 22 shows the Mach number at all the grid points. The sonic point on the wall has been observed to be far upstream of the throat, which indicates that higher heating rate occurs farther upstream of the throat than that expected from the simple one-dimensional analysis. This partially explains why, in past full-scale firings, the Titan III motor nozzle was ablated much more in a region far upstream of the throat than at the throat. Cold-flow tests were recently conducted at the Chemical Systems Division of United Technology Corporation for the 6° canted Titan III solid rocket motor using nitrogen with  $\gamma = 1.4$ ; the wall Mach number at the throat was measured<sup>27</sup> to be 1.52 which agrees fairly well with the computed value 1.6 for the axisymmetric nozzle.

<sup>26</sup> Private communication with Chemical Systems Division of United Technology Corporation on Titan III Engineering Drawings, Nov. 1978.

<sup>27</sup> Private communication with R. Dunlap, Chemical Systems Division of United Technology Corporation, Nov. 1978.

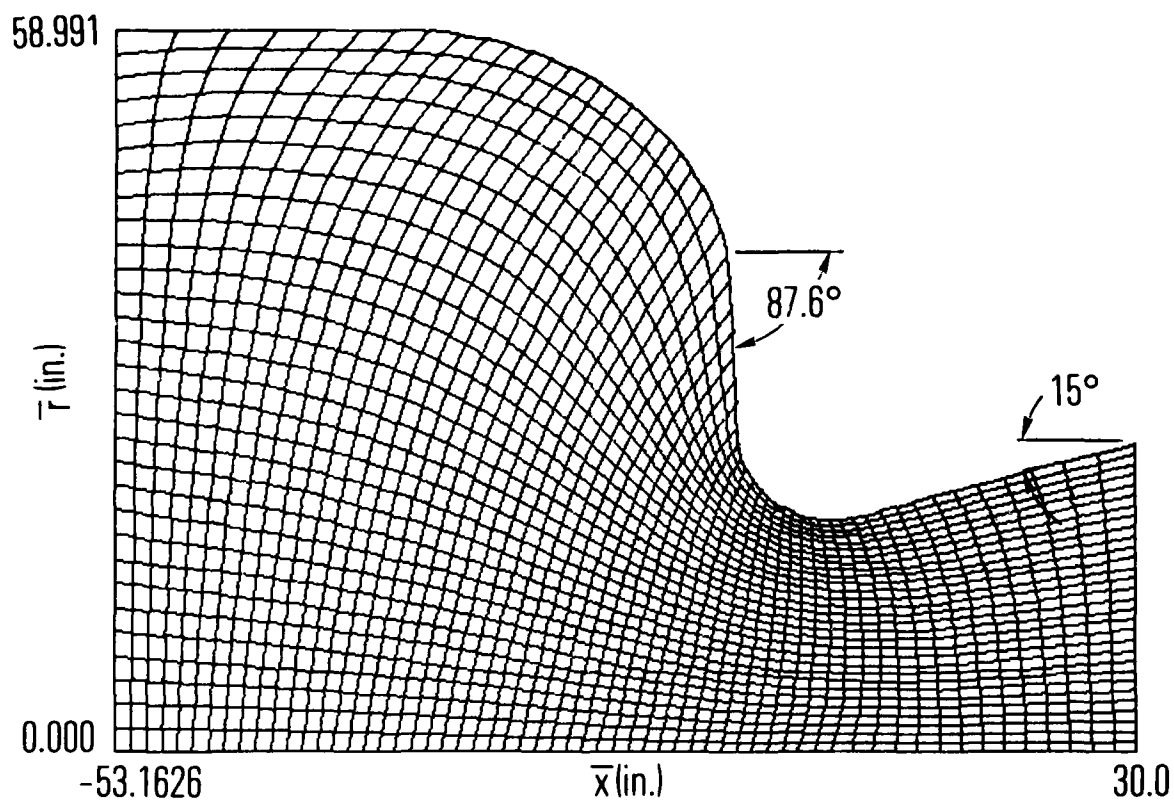


Fig. 18. BFC Grid for Steep Entrance Nozzle

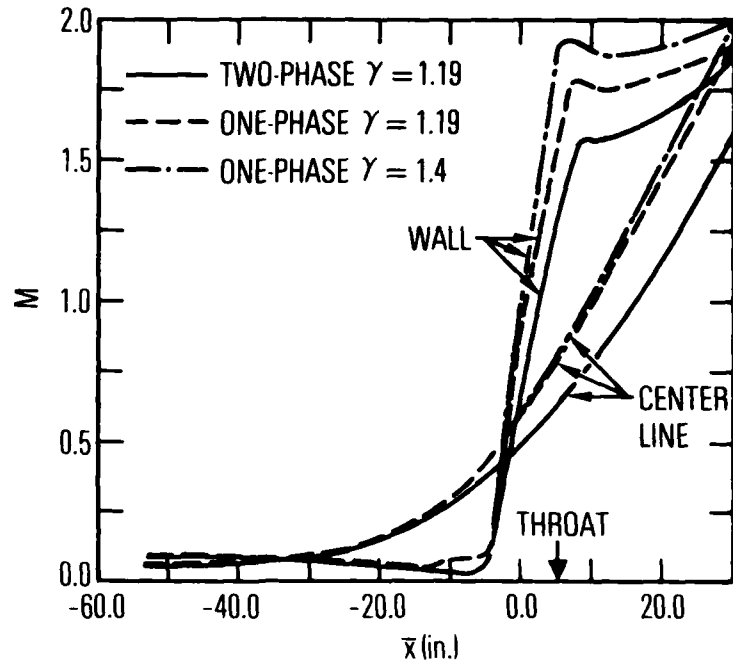


Fig. 19. Mach Number Distribution at Wall and Centerline for Steep Entrance Nozzle

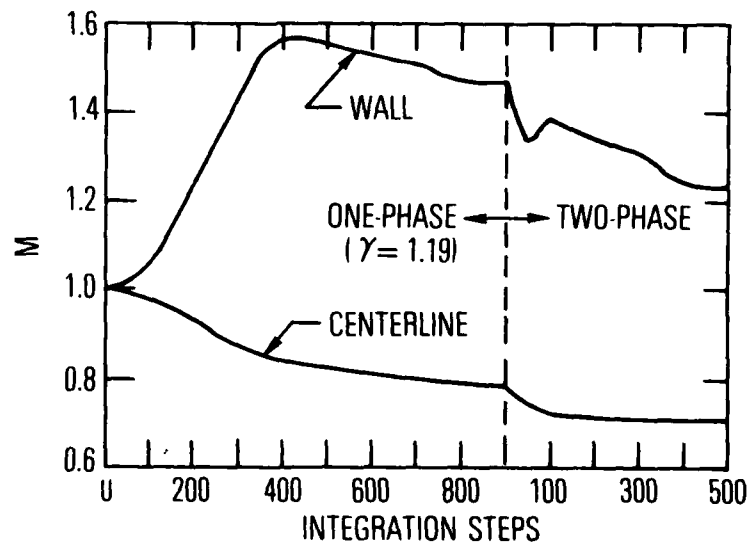


Fig. 20. Throat Mach Number at Every Integration Step for Steep Entrance Nozzle

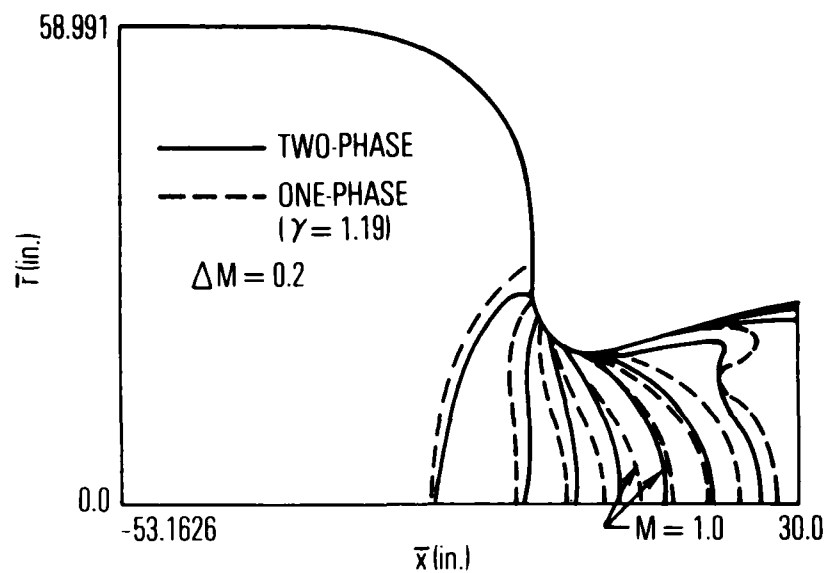


Fig. 21. Mach Number Contour for Steep Entrance Nozzle

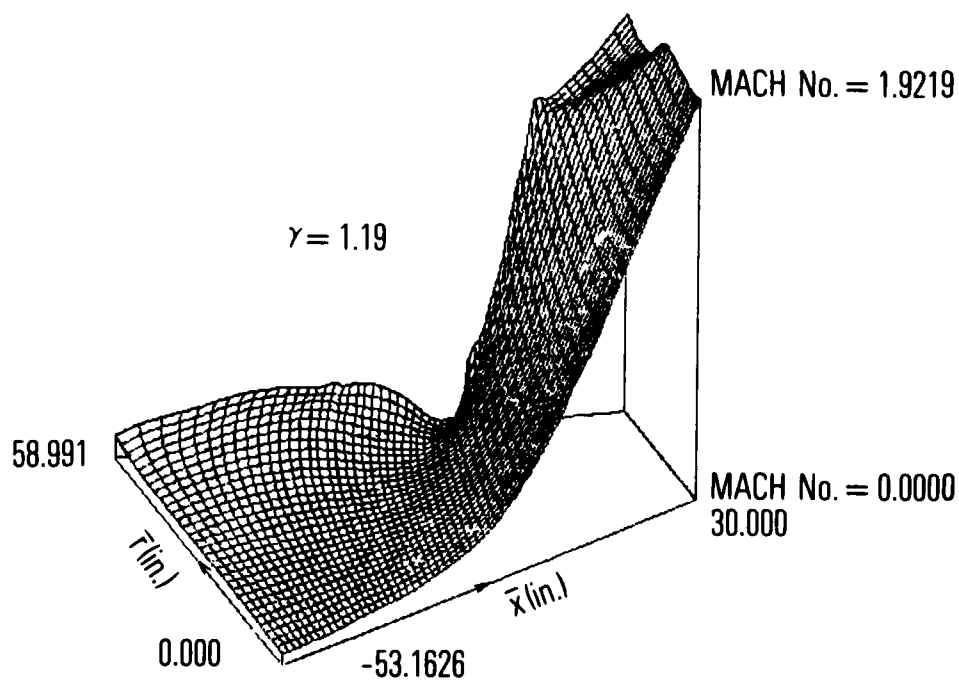


Fig. 22. Mach Number Pictorial Plot for Steep Entrance Nozzle (One-Phase Flow)

Note that no converged solution is possible with the conventional grid with vertical axial stations, such as that used in Refs. 4 through 8 and in most of the nozzle studies reported thus far, for the nozzle with a steep wall slope like that of the Titan III motor. It is the author's experience that when the nozzle wall slope is greater than  $\approx 60^\circ$ , the conventional grid with vertical axial station cannot handle the drastic change in flow properties along the steep wall, and this results in numerical instability. On the contrary, no difficulty is encountered in the calculation with the grid generated from the boundary-fitted coordinates system.

#### B. TWO-PHASE FLOW

The two-phase flow data for the Titan III motor are as follows:

<u>Gas Phase</u>	<u>Particle Phase</u>
$\bar{C}_p = 0.64 \text{ Btu/lb}_m\text{-}^\circ\text{R}$	$\bar{C}_j = 0.33 \text{ Btu/lb}_m\text{-}^\circ\text{R}$
$\bar{\mu}_{t1} = 5.97 \times 10^{-5} \text{ lb}_m/\text{ft-sec}$	$\bar{m}_j = 200 \text{ lb}_m/\text{ft}^3$
$P_r = 0.45$	$\bar{r}_j = 6\mu$
$A = 0.664, \gamma = 1.19$	$W_j/W_m = 28.8\%$

The chamber condition is  $\bar{T}_{t1} = 5890^\circ\text{R}$ ,  $\bar{P}_{t1} = 600 \text{ psia}$ .

The variation of the computed throat gas-phase Mach number along the wall and at the centerline at every integration step based on the initial guess from the previously computed one-phase results is also illustrated in Fig. 20. At the end of 500 integration steps the gas-phase Mach number distribution is shown in Fig. 19 for comparison with that of one-phase flow. The gas-phase Mach number contour is plotted in Fig. 21 and the corresponding gas-phase Mach number distribution throughout the flow field is depicted in Fig. 23.



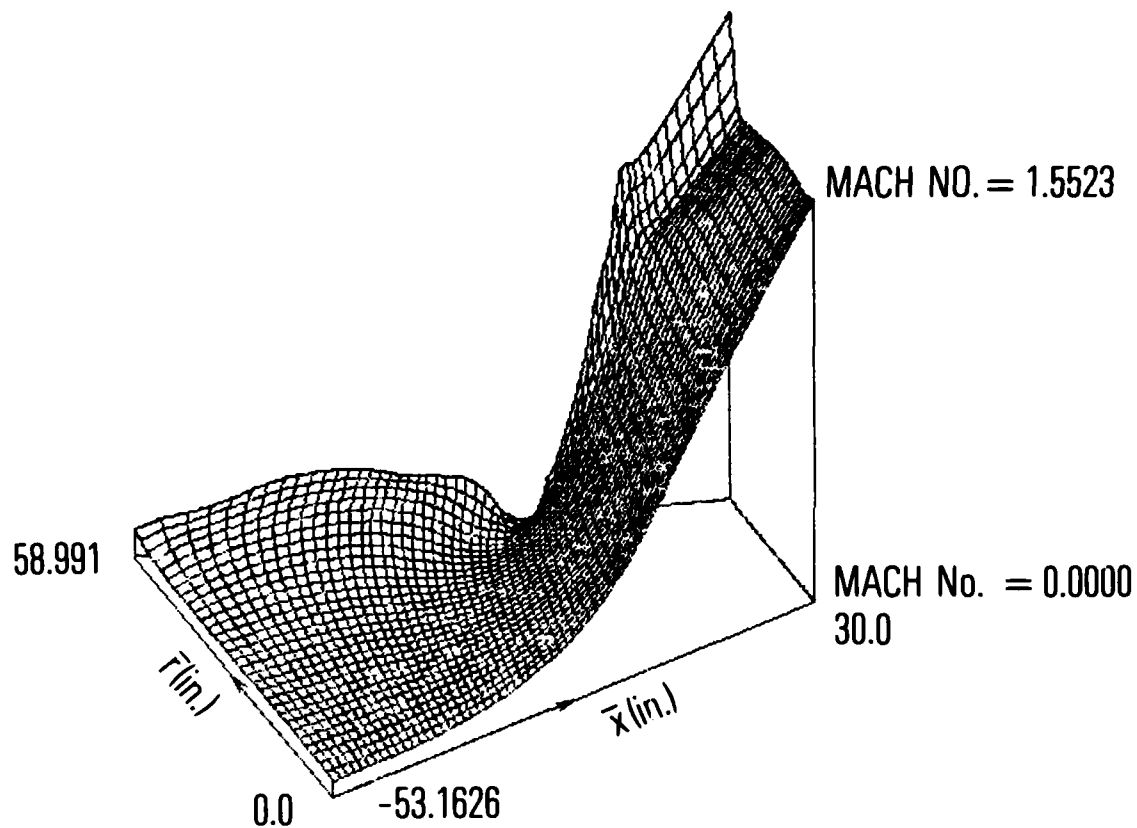


Fig. 23. Mach Number Pictorial Plot for Steep Entrance Nozzle (Two-Phase Flow)

The particle density contour and distribution are plotted in Figs. 24 and 25. The gas-phase pressure field has not been altered much by the introduction of particles in the flow field, and the pressure distribution is shown in Fig. 26. The velocity and temperature ratio are indicated in Fig. 27. The calculation of 500 integration steps for the two-phase flow takes 10 min, 37 sec execution time on the CDC 7600 computer.

Particles are likely to impinge on the steep wall in the entrance region. The present analysis does not incorporate any pertinent particle impingement model for calculating the erosion caused by such impingement. Nevertheless, the particle density contour obtained from this study does show regions of high particle concentration which may affect the results from boundary layer calculations and thereby the results of transient in-depth thermal analyses for the prediction of nozzle wall temperature.

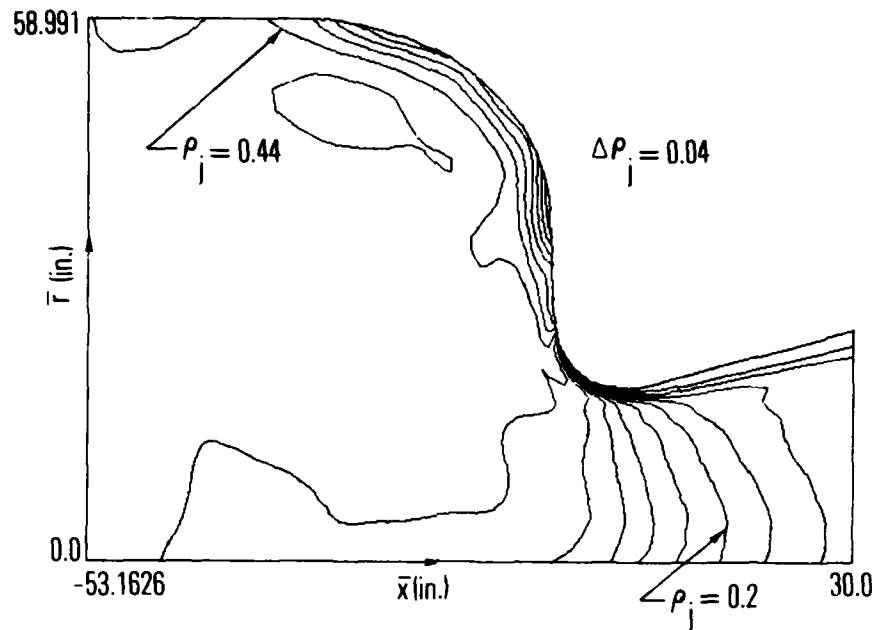


Fig. 24. Particle Density Contour for Steep Entrance Nozzle

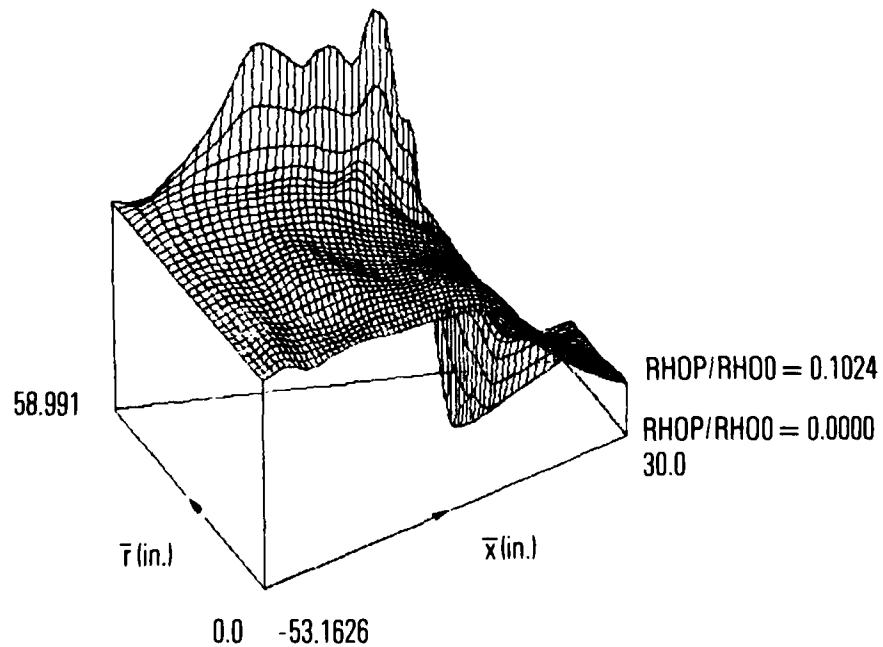


Fig. 25. Particle Density Pictorial Plot for Steep Entrance Nozzle

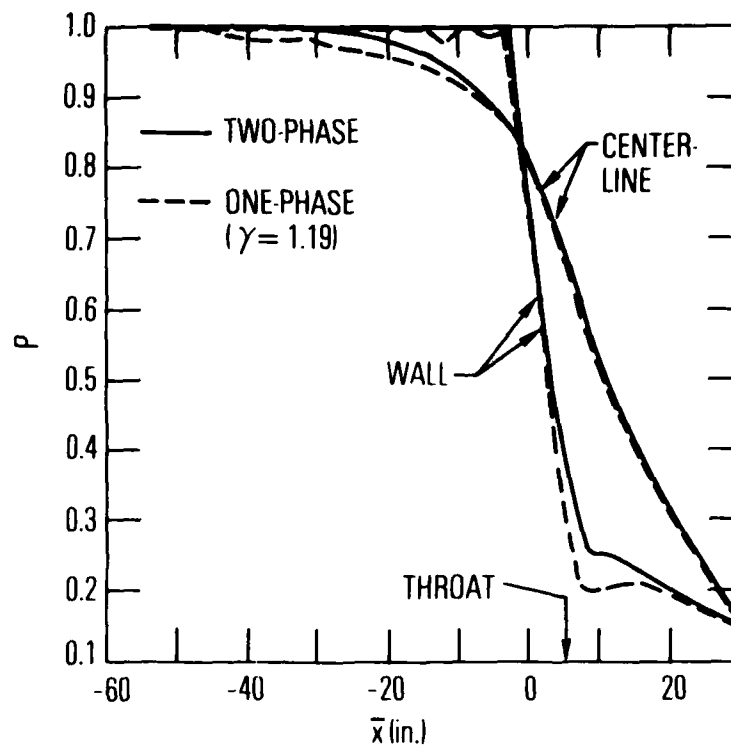


Fig. 26. Pressure Distribution for Steep Entrance Nozzle

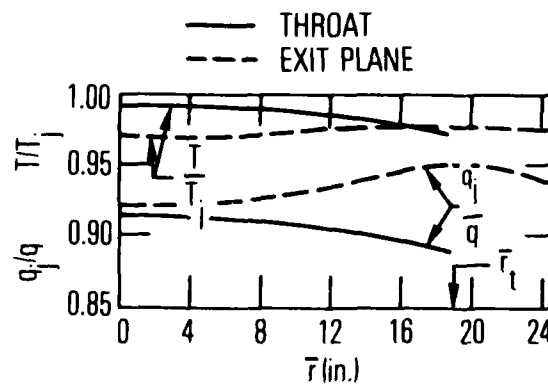


Fig. 27. Velocity Lag and Temperature Ratio for Steep Entrance Nozzle

## VI. SUBMERGED NOZZLE--IUS SMALL MOTOR

### A. ONE-PHASE FLOW

It has long been recognized that the solution of the flow field inside rocket motors with a submerged nozzle configuration constitutes an important phase of the flow-field study. Both large and small IUS solid rocket motors<sup>28</sup> have a submerged nozzle. The IUS will be used as an upper stage for both the Titan III and the Shuttle. In the past, due to the difficulty of analyzing the internal flow field for IUS-like motors with complicated geometry, various approximations have been adopted, and the accuracy of the pressure and heat transfer predictions on the submerged nozzle surface was therefore uncertain. Although the viscous effect would probably dominate some part of the submerged flow region in the gas-only one-phase flow, the inviscid flow solution shown here constitutes a first attempt toward a complete viscous flow solution in future studies.

The IUS small motor interior geometry including the igniter, submerged nozzle block, and a propellant burning surface is illustrated in Fig. 28, where the physical region for computation has been identified by heavy solid lines. The grid generated from the boundary-fitted coordinates system is depicted in Fig. 29. The flow region is bounded by: (a) the motor case, (b) the motor centerline of symmetry, (c) the igniter surface, (d) the supersonic exit plane, and (e) the propellant surface with radial mass inflow. The region depicted in Fig. 29 incorporates the entire subsonic flow region without introducing a fictitious vertical inlet boundary. The blowup figure for the submerged and throat region is shown in Fig. 30.

The propellant burning rate for the small IUS solid rocket motor is found to be 0.206 in/sec at  $\bar{T}_{t1} = 5985^\circ\text{R}$  and  $\bar{P}_{t1} = 410$  psia, which results in

<sup>28</sup>"Inertial Upper Stage SRM-II Baseline Design Review," Chemical Systems Division of United Technology Corporation, Dec. 1978.

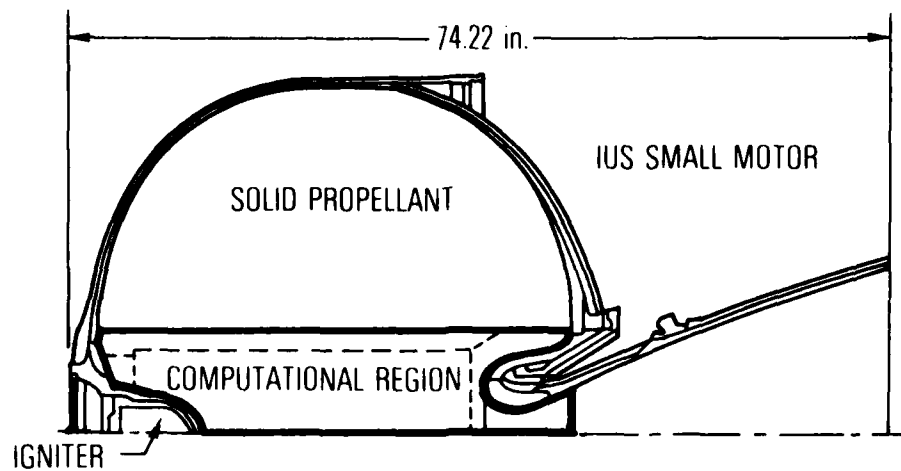


Fig. 28. IUS Small Motor Interior Configuration and Computational Region

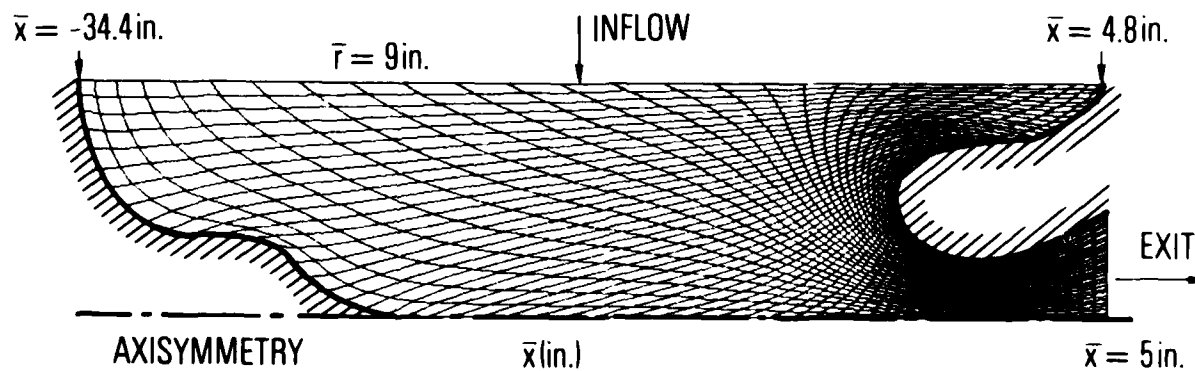


Fig. 29. BFC Grid for Small IUS SRM with Submerged Nozzle Block

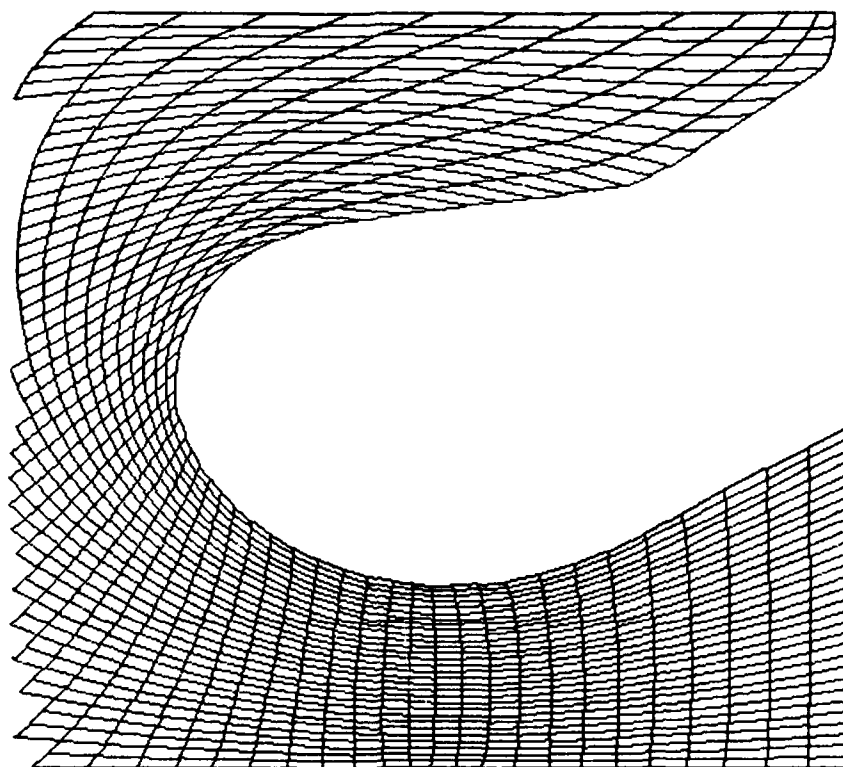


Fig. 30. Blown-up BFC Grid in the Submerged and Throat Region for Small IUS SRM

the fixed inlet condition at the propellant burning surface  $\bar{v} = 11.53$  ft/sec ( $M = 0.00322$ ) for  $\bar{C}_p = 0.45$  Btu/lb<sub>m</sub>-°R and  $\gamma = 1.19$ . The Mach number in the junction region, where the igniter joins the zero radius centerline, was computed incorrectly in an earlier study. In this report, the boundary points with the radial coordinate smaller than the radial length of the adjacent finite difference mesh are treated as the centerline points of zero radius, and L'Hospital's rule is conveniently applied thereby avoiding numerical error resulting from decoding conservative variables divided by a very small number (small radial coordinate).

Unlike the previous two nozzle flows, a stricter convergence criterion is deemed necessary for the submerged nozzle calculation and requires that the difference in Mach number be less than 0.001% and in mass flow rate less than 0.001% at the throat for three consecutive integration steps. For the 61 x 31 grid points shown in Fig. 29, the converged solution requires 4487 integration steps and takes 38 min, 16 sec execution time on the CDC 7600 computer.

Figure 31 indicates the computed throat Mach number at every integration step. The IUS solid rocket motor has a throat with a large radius of curvature; the computed Mach number at the throat is 1.071 on the wall and 0.947 at the centerline which are close to a uniform one-dimensional flow. Figure 32 depicts the Mach number distribution along the boundary, while the computed Mach number contour is plotted in Fig. 33. Figure 34 shows the velocity vector plot in the submerged and throat region.

#### B. TWO-PHASE FLOW

The following data are used for the two-phase flow inside the small IUS motor:



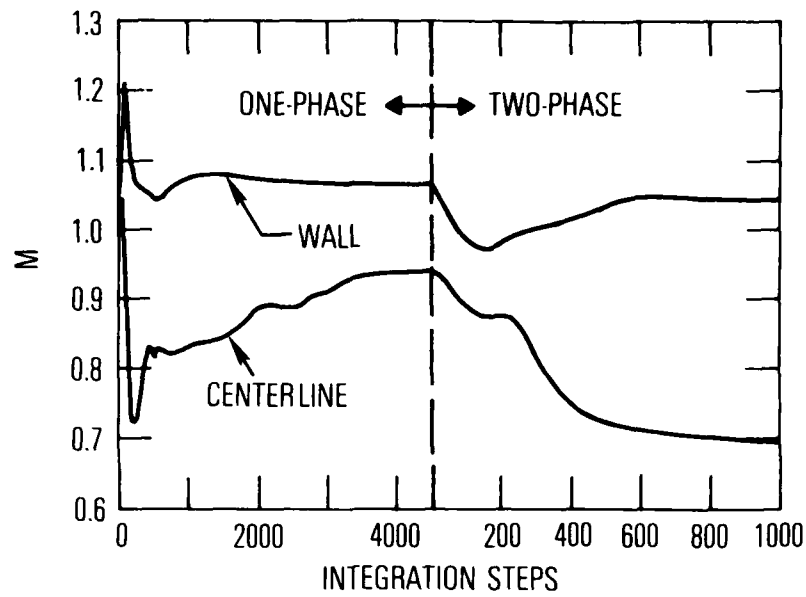


Fig. 31. Throat Mach Number at Every Integration Step for Small IUS SRM

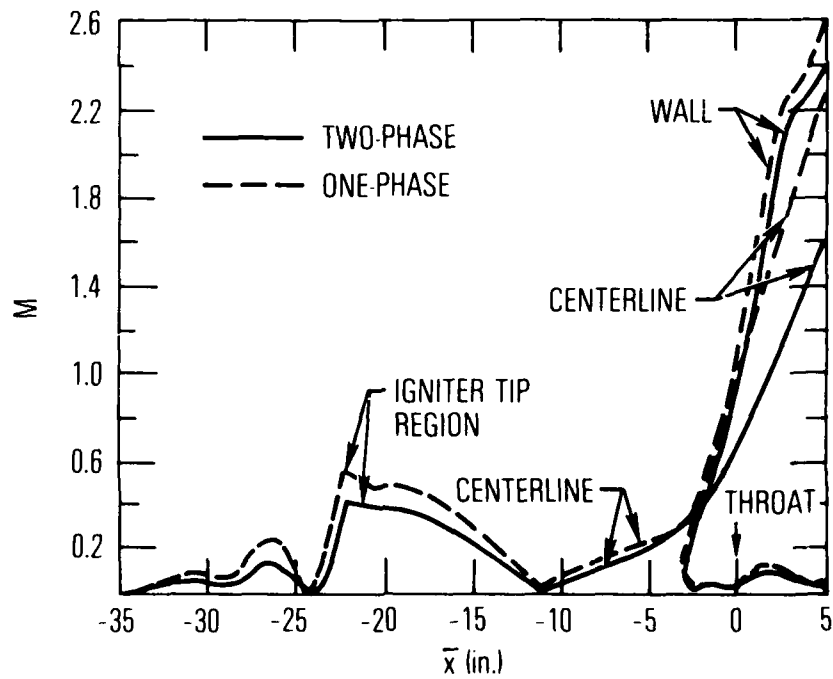


Fig. 32. Mach Number Distribution on the Boundary for Small IUS SRM Nozzle

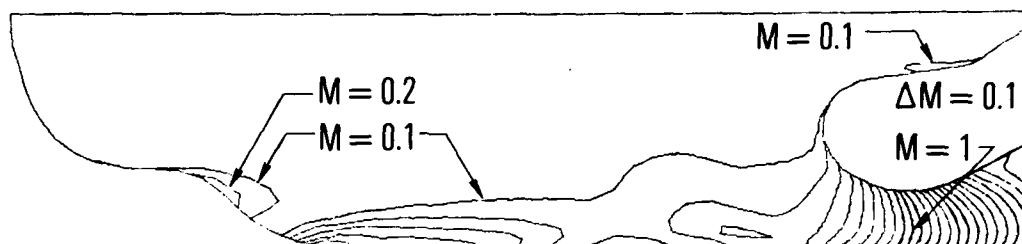


Fig. 33. Mach Number Contour for Small IUS SRM  
(One-Phase Flow)

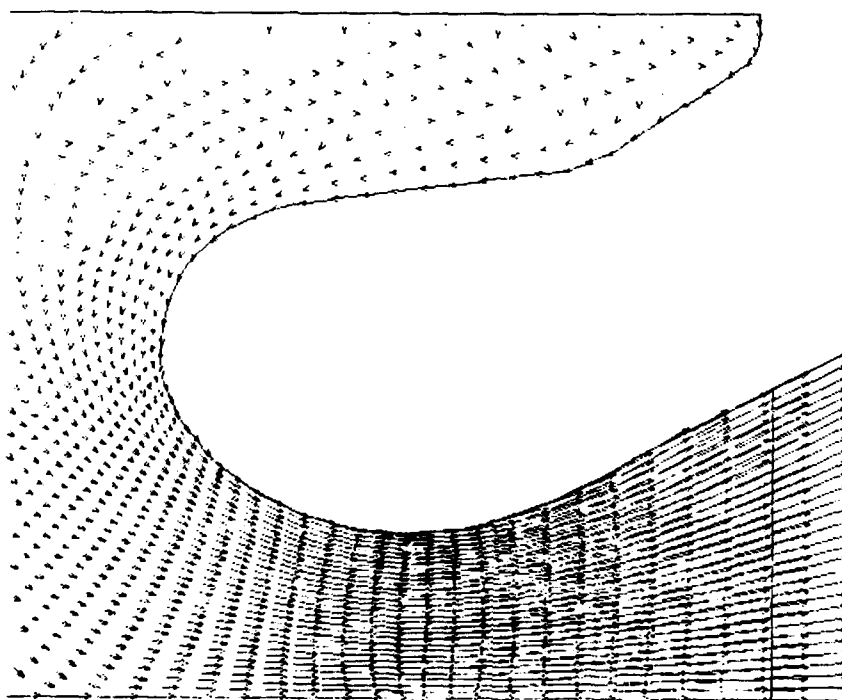


Fig. 34. Velocity Vector Plot in the Submerged and Throat  
Region for Small IUS SRM (One-Phase Flow)

<u>Gas Phase</u>	<u>Particle Phase</u>
$\overline{C}_p = 0.45 \text{ Btu/lb}_m\text{-}^\circ\text{R}$	$\overline{C}_j = 0.32 \text{ Btu/lb}_m\text{-}^\circ\text{R}$
$\overline{\mu}_{t1} = 5.674 \times 10^{-5} \text{ lb}_m/\text{ft-sec}$	$\overline{m}_j = 200 \text{ lb}_m/\text{ft}^3$
$P_r = 0.269$	$\overline{W}_j/\overline{W}_m = 30\%$
$A = 0.65$	$\overline{r}_j = 2.5\mu$
$\gamma = 1.19$	

The chamber condition is  $\overline{T}_{t1} = 5985^\circ\text{R}$ ,  $\overline{P}_{t1} = 410 \text{ psia}$ .

The throat Mach number at every integration step is shown in Fig. 31 for easy comparison with the one-phase solution. The Mach number distribution along the boundary surface is indicated in Fig. 32. The gas-phase Mach number at exit plane is 1.57 at centerline and 2.41 at wall for the two-phase flow; these are smaller than the corresponding Mach numbers of 2.25 and 2.57 found in the gas-only one-phase flow, due to the presence of solid particles in the flow field. This implies that an IUS solid rocket motor nozzle flow field and heat transfer analysis based solely on a gas-only one-phase study will be in error. Figure 35 shows the gas-phase and Fig. 36 the particle velocity vector plot. A distinctive particle-free zone is visible from the particle velocity vector plot of Fig. 36. Figure 37 is the computed gas-phase Mach number contour, and Fig. 38 is the particle density contour in the two-phase flow. The velocity lag and gas-to-particle temperature ratio at throat (where  $\overline{r}_t = 2.15 \text{ in.}$ ) and exit plane (where  $\overline{r}_e = 4.05 \text{ in.}$ ) are shown in Fig. 39.

Although the submerged nozzle configuration is complex and the governing two-phase partial differential equations are highly nonlinear, no computational difficulty has been encountered during the course of this study, and the

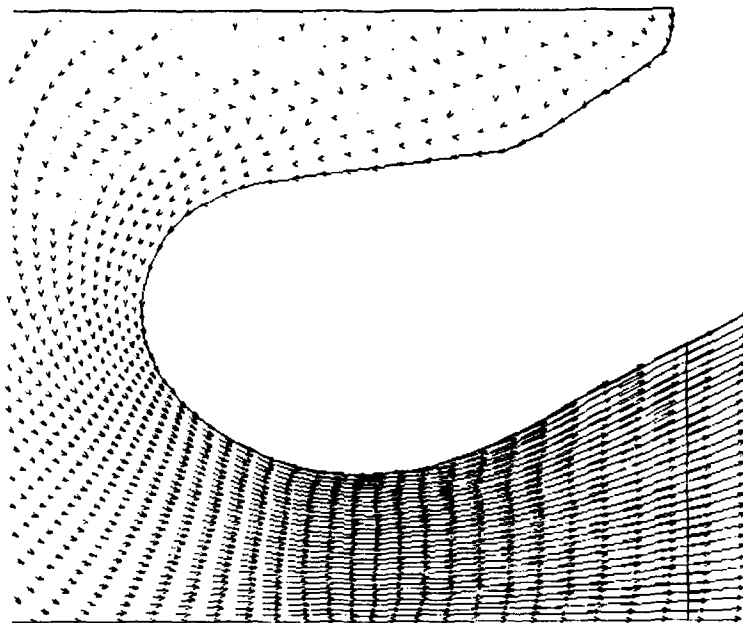


Fig. 35. Gas-Phase Velocity Vector Plot in the Submerged and Throat Region for Small IUS SRM (Two-Phase Flow)

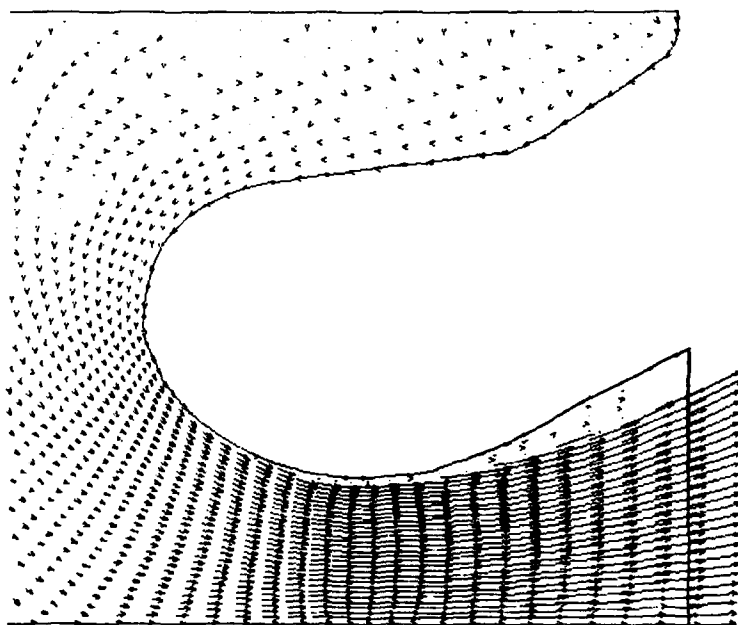


Fig. 36. Particle Velocity Vector Plot in the Submerged and Throat Region for Small IUS SRM (Two-Phase Flow)

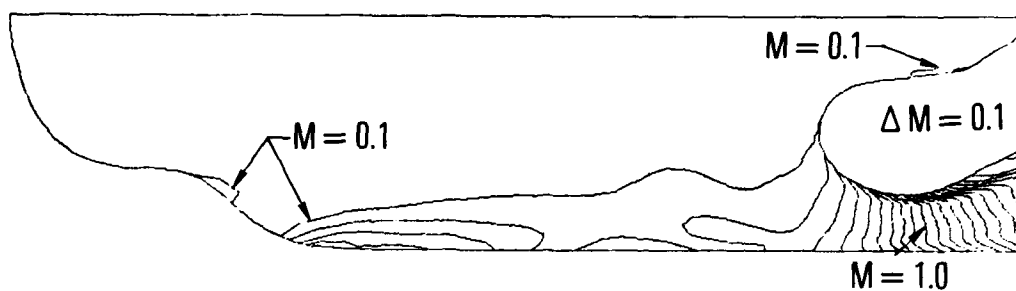


Fig. 37. Gas-Phase Mach Number Contour for Small IUS SRM (Two-Phase Flow)



Fig. 38. Particle Density Contour for Small IUS SRM (Two-Phase Flow)

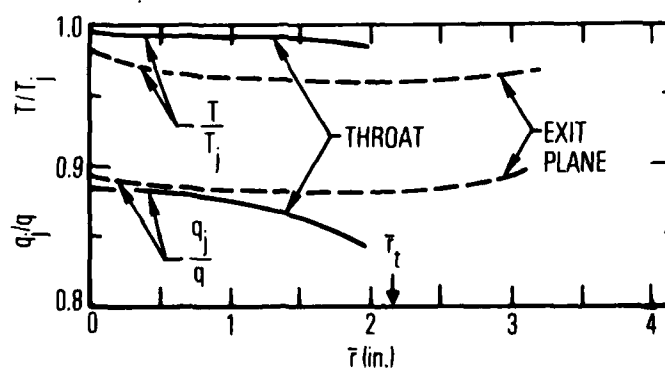


Fig. 39. Velocity Lag and Temperature Ratio for Small IUS SRM

timewise integration has been carried out in a straightfoward manner. For the submerged small IUS solid rocket motor nozzle, the two-phase flow field calculation of 1000 integration steps takes 23 min, 2 sec execution time on the CDC 7600 computer. All the two-phase flow features mentioned previously for the JPL and Titan III nozzle are equally applicable to this submerged IUS solid rocket motor nozzle.

## VII. CONCLUDING REMARKS

The following conclusions have been reached as a result of this study:

- a. A time-dependent technique with the MacCormack finite difference scheme provides stable integration for both one- and two-phase nozzle flow equations.
- b. The utilization of the BFC system enhances the capability of the program to the solution of flow inside nozzles with complex geometry.
- c. Imbedded shock can occur in the region downstream of the nozzle geometric throat for the flow inside nozzle with small throat radius of curvature.
- d. The small-sized particles act more effectively to slow down the gas-phase expansion than that of large-sized particles for the same particle mass fraction.
- e. For a two-phase flow with high particle loading ratio, the gas-phase can become subsonic at the geometric throat.
- f. The computed one- and two-phase results are important for nozzle wall heat transfer and ablation study.
- g. In general, the assumption of constant fractional lag is not justified for a two-phase transonic flow. The prediction of the gas-particle flow field requires that the proper momentum and energy exchange between the gas and particles, such as the fully coupled solution presented in this study, be taken into account.

## REFERENCES

1. Hopkins, D. E. and D. E. Hill, "Effect of Small Radius of Curvature on Transonic Flow in Axisymmetric Nozzles," AIAA J., 4(8), Aug. 1966, p. 1337.
2. Kliegel, J. R. and V. Quan, "Convergent-Divergent Nozzle Flows," AIAA J., Sept. 1968, p. 1728.
3. Prozan, R. J., reported in "Numerical Solution of the Flowfield in the Throat Region of a Nozzle," by L. M. Saunders, BSVD-P-66TN-001 (NASA CR82601), Aug. 1966, Brown Engineering Co., Huntsville, Ala.
4. Migdal, D., K. Klein, and G. Moretti, "Time-Dependent Calculations for Transonic Nozzle Flow," AIAA J., 7(1), Feb. 1969, p. 372.
5. Wehofer, S. and W. C. Moger, "Transonic Flow in Conical Convergent and Convergent-Divergent Nozzles with Nonuniform Inlet Conditions," AIAA Paper No. 70-635.
6. Laval, P., "Time-Dependent Calculation Method for Transonic Nozzle Flows," Lecture Notes in Physics, 8, Jan. 1971, p. 187.
7. Serra, R. A., "Determination of Internal Gas Flows by a Transient Numerical Technique," AIAA J., 10(5), May 1972.
8. Cline, M. C., "Computation of Steady Nozzle Flow by a Time-Dependent Method," AIAA J., 12(4), Apr. 1974, p. 419.
9. Brown, E. F. and G. L. Hamilton, "A Survey of Methods for Exhaust-Nozzle Flow Analysis," AIAA Paper No. 60, 1975.
10. Hoglund, R. F., "Recent Advances in Gas-Particle Nozzle Flows," ARS Journal, May 1962, p. 662.
11. Regan, J. F., H. D. Thompson, and R. F. Hoglund, "Two-Dimensional Analysis of Transonic Gas-Particle Flows in Axisymmetric Nozzles," J. Spacecraft, 8(4), Apr. 1971, p. 346.
12. Jacques, L. J. and J. A. M. Seguin, "Two-Dimensional Transonic Two-Phase Flow in Axisymmetric Nozzles," AIAA Paper No. 74-1088, Oct. 1974.



#### REFERENCES (Continued)

13. Kliegel, J. R. and G. R. Nickerson, "Axisymmetric Two-Phase Perfect Gas Performance Program," Report 02874-6006-R000, Vols. I and II, Apr. 1967, TRW Systems Group, Redondo Beach, Ca. 90278.
14. Coats, D. E., et al., "A Computer Program for the Prediction of Solid Propellant Rocket Motor Performance," Vols. I, II, and III, AFRPL-TR-75-36, July 1975.
15. Soo, S. L., "Gas Dynamic Processes Involving Suspended Solids," A.I.Ch.E. Journal, 7(3), Sept. 1961, p. 384.
16. Hultberg, J. A. and S. L. Soo, "Flow of a Gas-Solid Suspension Through a Nozzle," AIAA Paper No. 65-6, Jan. 1965.
17. Thompson, J. F., F. C. Thames, and C. W. Martin, "Boundary-Fitted Curvilinear Coordinates Systems for Solution of Partial Differential Equations on Fields Containing Any Number of Arbitrary Two-Dimensional Bodies," NASA CR 2729, July 1977.
18. Henderson, C. B., "Drag Coefficients of Spheres in Continuum and Rarefied Flows," AIAA J., 14(6), June 1976, p. 707.
19. Carlson, D. J. and R. F. Hoglund, "Particle Drag and Heat Transfer in Rocket Nozzles," AIAA J., 2(11), 1964, p. 1980.
20. MacCormack, R. W., "The Effect of Viscosity in Hypervelocity Impact Cratering," AIAA Paper 69-354, May 1969.
21. Chang, I-Shih, "Three-Dimensional Supersonic Internal Flows," AIAA Paper 76-423, July 1976.
22. Kutler, P., L. Sakell, and G. Aiello, "On the Shock-on-Shock Interaction Problem," AIAA Paper No. 74-524, June 1974.
23. Cuffel, R. F., L. H. Back, and P. F. Massier, "Transonic Flowfield in a Supersonic Nozzle with Small Throat Radius of Curvature," AIAA J., 7(7), July 1969, p. 1364.
24. Chow, W. L. and I-Shih Chang, "Mach Reflection Associated with Over-expanded Nozzle Free Jet Flows," AIAA J., 13(6), June 1975.
25. Chang, I-Shih and W. L. Chow, "Mach Disc from Underexpanded Axisymmetric Nozzle Flow," AIAA J., 12, Aug. 1974, p. 1079.

#### REFERENCES (Concluded)

26. Private communication with Chemical Systems Division of United Technology Corporation on Titan III Engineering Drawings, Nov. 1978.
27. Private communication with R. Dunlap, Chemical Systems Division of United Technology Corporation, Nov. 1978.
28. "Inertial Upper Stage SRM-II Baseline Design Review," Chemical Systems Division of United Technology Corporation, Dec. 1978.

DATE  
FILMED  
— 8